JGR Solid Earth

RESEARCH ARTICLE
10.1029/2022JB025562

Key Points:

- Parental magmas of high-Al chromitites were derived from hydrous harzburgitic mantle
- High-Al chromitites formed at the early stage of flux melting during subduction initiation
- The δ^7Li variation of olivine in dunites reveals a period of sluggish slab rollback

Supporting Information:

Supporting Information may be found in the online version of this article.

Correspondence to:

P.-F. Zhang and M.-F. Zhou,
zhangpengfei073061@163.com;
zhoumeifu@hotmail.com

Citation:

Zhang, P.-F., Zhou, M.-F., Liu, Q.-Y., Malpas, J., Yumul, G. P. Jr., & Wang, C. Y. (2023). Sluggish slab rollback at the early stage of flux melting during subduction initiation: Li isotopic evidence from the Coto high-Al chromite deposit, Zambales ophiolite, Philippines. *Journal of Geophysical Research: Solid Earth*, *128*, e2022JB025562. https://doi.org/10.1029/2022JB025562

Received 8 SEP 2022
Accepted 1 MAR 2023

Author Contributions:

Conceptualization: Peng-Fei Zhang, Mei-Fu Zhou, John Malpas, Graciano P. Yumul Jr.
Formal analysis: Peng-Fei Zhang
Funding acquisition: Peng-Fei Zhang, Mei-Fu Zhou, Christina Yan Wang
Investigation: Peng-Fei Zhang, Mei-Fu Zhou, Graciano P. Yumul Jr.
Methodology: Peng-Fei Zhang
Project Administration: Peng-Fei Zhang
Software: Qiong-Ying Liu
Validation: Peng-Fei Zhang
Writing – original draft: Peng-Fei Zhang, Graciano P. Yumul Jr.
Writing – review & editing: Peng-Fei Zhang, Mei-Fu Zhou, John Malpas, Graciano P. Yumul Jr., Christina Yan Wang

Sluggish Slab Rollback at the Early Stage of Flux Melting During Subduction Initiation: Li Isotopic Evidence From the Coto High-Al Chromite Deposit, Zambales Ophiolite, Philippines

Peng-Fei Zhang[1,2], Mei-Fu Zhou[1,3], Qiong-Ying Liu[4], John Malpas[5], Graciano P. Yumul Jr.[6], and Christina Yan Wang[2]

[1]State Key Laboratory of Geological Processes and Mineral Resources, China University of Geosciences, Wuhan, China, [2]CAS Key Laboratory of Mineralogy and Metallogeny, Guangzhou Institute of Geochemistry, Chinese Academy of Sciences, Guangzhou, China, [3]State Key Laboratory of Ore Deposit Geochemistry, Institute of Geochemistry, Chinese Academy of Sciences, Guiyang, China, [4]Institute of Geology, China Earthquake Administration, Beijing, China, [5]Department of Earth Sciences, The University of Hong Kong, Hong Kong, China, [6]Cordillera Exploration Company, Inc., Taguig, Philippines

Abstract The compositions of chromitites and dunites from Moho transition zone (MTZ) of the Coto block of the Zambales ophiolite, Philippines, are used to investigate the geodynamic transition from anhydrous to hydrous magmatism during subduction initiation (SI). Chromite grains in the chromitites have Cr# values [100 × Cr/(Cr + Al)] and TiO_2 contents ~35–50 and 0.05–0.30 wt.%, respectively, intermediate between those of chromite in typical MORB-like lavas (Cr#, ~20–60; TiO_2, ~0.6–1.7 wt.%) and boninites (Cr#, ~70–85; TiO_2, <0.4 wt.%). Olivine grains in the dunites have δ^7Li values varying from ~−2‰ to +21‰ with most between +10‰ and +15‰, beyond that of normal mantle (+4 ± 2‰) but comparable to those of some arc lavas (up to +12‰). The data set indicates that parental magmas of the high-Al chromitites originated from hydrated harzburgitic mantle sources and formed temporally between MORB-like and boninitic magmatism during SI, resulting from the early stage of flux melting in the Zambales proto-forearc mantle. Modeling of Li diffusion reveals that the MTZ cooled down at a minimum rate of 0.1°C/yr in order to preserve the large δ^7Li variation of olivine in the dunites, comparable to the thermal conditions below ultra-slow to slow spreading ridges. Such a stage of transitional magmatism, although displaying notable slab contributions, took place at a sluggish period of slab rollback and asthenospheric upwelling, leading to a trough level of heat flow and magma production during the entire course of SI.

Plain Language Summary Subduction initiation (SI) is a prerequisite for starting plate movement. It is featured by rollback of subducted oceanic slabs in the mantle and upward flow of deep mantle materials into the shallow mantle wedges, resulting in mid-ocean ridge-like spreading settings above the retreating slabs and mid-ocean ridge basalt-like (MORB-like) lavas. Heated by surrounding hot mantle, slabs gradually release fluids into the overlying mantle, inducing H_2O-rich magmatism such as boninitic ones. Although MORB-like and boninitic lavas are accepted to originate from H_2O-poor and H_2O-rich mantle sources, respectively, few details were revealed on how transition between the two contrasting types of magmatism is achieved. This work did chemical analyses and modeling on some SI-related rocks that show affinity to transitional MORB-boninitic magmatism. Our results show the transitional magmas originated from mantle sources chemically similar to those of boninites, but formed under cooler conditions than both MORB-like and boninitic lavas. Development of such transitional magmatism reveals that the sources of SI-related magmas became increasingly rich in fluids, and there was a cooling period between the MORB and boninitic magmatism, possibly due to slow slab rollback and sluggish upwelling of deep hot mantle below the SI-induced spreading centers during the transitional period.

1. Introduction

Intra-oceanic subduction plays a major role in driving the motion of lithospheric plates, and knowledge of how subduction is initiated and evolves is fundamental to our understanding of global tectonic and magmatic processes. Subduction initiation (SI) has been considered to be featured by proto-forearc spreading above descending slabs and magma production that varies from early MORB-like forearc basalts (FAB) to later boninites generally in

several Myrs (Maunder et al., 2020; Reagan et al., 2010, 2019; Stern et al., 2012; Waldman et al., 2021; Whattam & Stern, 2011). Although the FAB and boninitic magmatism have been well explained as the results of decompressional melting of asthenosphere and hydrous melting of harzburgitic mantle below proto-forearc spreading centers, respectively (Stern et al., 2012; Whattam & Stern, 2011), the geochemical transition and associated slab dynamics between the two types of magmatism remain poorly understood. Consequently, our knowledge of the overall geodynamic evolution of subduction initiation is limited.

Examples of contemporary SI are rare, and historical in situ cases are often subject to modification by subsequent tectonic or crust-forming events (Arculus et al., 2019; Patriat et al., 2019; Stern et al., 2012), making it challenging to acquire appropriate lava samples for studying SI. Supra-subduction zone (SSZ) ophiolites are increasingly recognized to be formed during SI (Casey & Dewey, 1984; Pearce, 2003; Stern, 2004; Stern et al., 2012; Whattam & Stern, 2011). Although most SSZ ophiolites do not have well-kept lava sequences due to tectonic destruction, their mantle sequences and Moho transition zones (MTZ) are often better preserved (C. Z. Liu et al., 2022; Robertson et al., 2013). In particular, chromitites and dunites are closely associated in the mantle sequences and MTZ of ophiolites, and were produced by Mg-rich magmatism via melt-peridotite reaction (replacive origin) and crystal accumulation (cumulate origin) (Arai, 1997; Arai & Yurimoto, 1994; P. F. Zhang et al., 2016; Zhou et al., 1994, 1998). Chromite grains in chromitites show a large Cr# variation from ∼15 to 85, and have been classified as high-Al (Cr# < 60) and high-Cr (Cr# > 60) varieties. Although high-Al and high-Cr chromitites are regarded as products of MORB-like and boninitic magmatism, respectively (Arai, 1997; Morishita et al., 2007, 2011; Uysal et al., 2009; Zhou et al., 1996), chromite grains in high-Al chromitites generally have Cr# similar to those in MORB-like lavas (∼20–60) and TiO_2 contents similar to those in boninites (<0.3 wt.%) (Kamenetsky et al., 2001; Uysal et al., 2009; González-Jiménez et al., 2011), suggesting that their parental magmas have transitional compositions between MORB-like and boninitic magmas (Chen et al., 2019; X. Liu et al., 2019; P. F. Zhang et al., 2020). Consequently, high-Al chromitites and their associated dunites are potentially useful for investigating the genesis of transitional FAB-boninitic magmatism and related geodynamic processes during SI.

The low concentrations of incompatible elements (e.g., Sr-Nd-Pb) in chromitites and dunites make it difficult to use traditional elemental and isotopic tools to explore the origins of these rocks. However, in-situ Li isotopic analysis and its application to mantle minerals (e.g., olivine) may help to solve the problem. Terrestrial materials have large Li isotopic variation, for example, the δ^7Li values of N-MORB and their mantle sources are $+4 \pm 2‰$, whereas altered oceanic crust has δ^7Li values ranging from $\sim -12‰$ to $+21‰$ (B. X. Su et al., 2016; Tang et al., 2010; Tomascak et al., 2016). Due to the high solubility of Li in fluids, fluids released from subducted oceanic slabs usually display higher Li concentrations (tens of ppm) and different Li isotopic features than normal mantle (unmodified by exotic components; Li, ∼1–2 ppm; δ^7Li, $+4 \pm 2‰$) (Benton et al., 2004; Ishikawa et al., 2005; Marschall et al., 2007; Ottolini et al., 2004; Pogge von Strandmann et al., 2011; Savov et al., 2007; Seitz & Woodland, 2000). Therefore, addition of slab-derived fluids appears an effective way of modifying Li isotopic features of mantle wedges. In addition to being used as geochemical tracers, the fast diffusivity of Li makes Li isotopes powerful geo-speedometers for estimating the cooling rates and timescales of rapid processes (Gao et al., 2011; Parkinson et al., 2007). Further, given that the cooling rates and magmatic spreading rates of oceanic ridges are overall negatively correlated, for example, $\sim 10^{-4}$ and 10^{-1}°C/yr for some fast and ultra-slow spreading ridges, respectively (Coogan et al., 2007; P. P. Liu et al., 2020; Schmitt et al., 2011; Schwartz et al., 2005), measurements of Li isotopes in olivine grains in chromitites and dunites may also help to elucidate the geodynamic evolution during SI.

The Zambales ophiolite, exposed in the NW Luzon, Philippines, is a fragment of SSZ oceanic lithosphere and is thought to have formed ∼43–45 Ma in the West Pacific during SI (Figures 1a and 1b; J. P. Encarnación et al., 1993; J. Encarnación et al., 1999; Geary et al., 1989; Perez et al., 2018). The Coto block of the ophiolite hosts the largest high-Al chromite deposit in the world (6.34 Mt; Figure 1c; Hock et al., 1986; Xiong et al., 2013). More particularly, massive chromitites in the deposit enclose fresh dunites (Figures 2a–2e). According to Payot et al. (2013), formation of the dunite enclaves was attributed to pervasive reactions between harzburgites and parental magmas of chromitites under conditions of high melt/rock ratios. Such feature has never been reported in other cases because peridotites that host high-Al chromite deposits mostly show extensive serpentinization (González-Jiménez et al., 2011; Robinson et al., 1999; Zhou et al., 2001). As a result, presence of such fresh dunite samples makes the Coto block a unique laboratory for exploring the origin of the high-Al chromitites and nature of relevant magmatism.

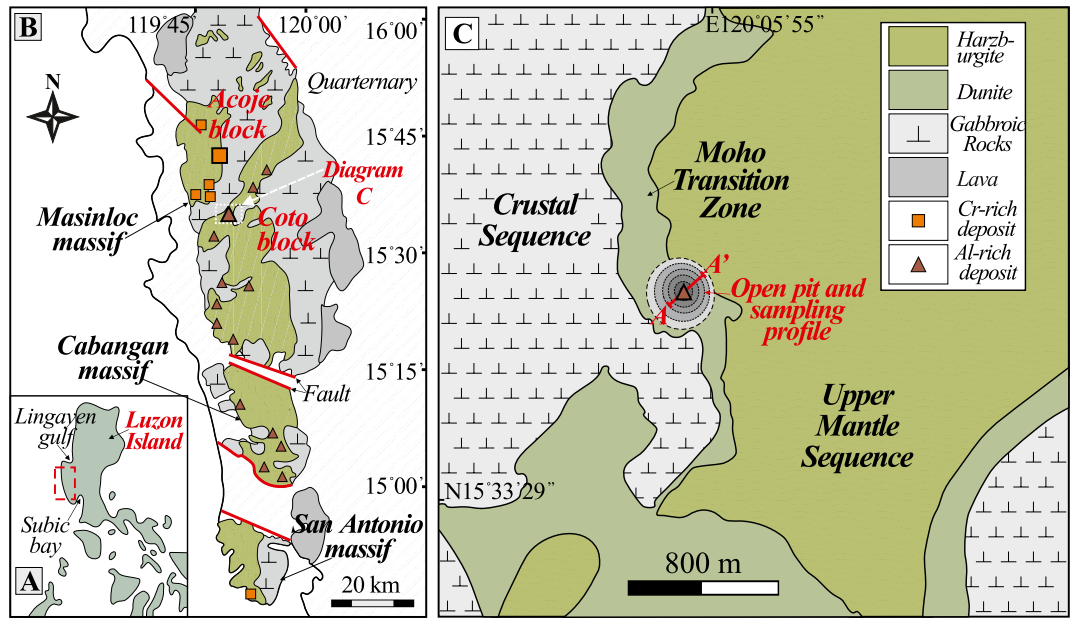

Figure 1. Locations and geological maps of the Zambales ophiolite and the Coto block. (a): Position of the Zambales ophiolite in the Luzon island, marked by the dashed red box. (b): Geological map of the Zambales ophiolite and distribution of all chromite deposits. Only harzburgites and gabbros are shown for the ultra-mafic and intrusive sequences in the diagram, due to the small volumes of dunites and other rocks in the ophiolite. (c): Geological map of the Coto block. The shaded concentric gray circles represent open pit of the Coto chromite deposit. Harzburgite, dunite and chromitite samples used in this study were all collected along the profile A-A', which strides the mantle-MTZ border of the block. Diagrams A and B are modified from Hock et al. (1986). Diagram (c) was mapped by Prof. Graciano P. Yumul Jr.'s research group.

In this study, we have undertaken in-situ Li isotopic analyses to olivine grains in the dunite enclaves, which is the first study of Li isotopes for high-Al chromite deposits. Combined with the compositions of chromite and numerical modeling, we investigate the origin of high-Al chromitites. Relevant discoveries are then used to reconstruct the geodynamic setting during the transitional FAB-boninitic magmatism and improve the current model of SI.

2. Geological Background

The Zambales ophiolite stretches from the Subic Bay in the south to the Lingayen Gulf in the north, over an area of ~4,500 km^2 (Figures 1a and 1b; Yumul et al., 1998). It is divided into the Masinloc, Cabangan, and San Antonio massifs from the north to south (Figure 1b). The Masinloc massif is further subdivided into the Coto block in the south and the Acoje block in the north, which host world-class high-Al and high-Cr chromite deposits, respectively (Figure 1b; Hock et al., 1986; Leblanc & Violette, 1983; Yumul et al., 1998).

Both the Coto and Acoje blocks show comparable architectures to mid-ocean ridges (MOR), for example, having sheeted dykes and pillow lavas (Yumul, 1996), indicating that the blocks were formed at MOR-like spreading settings rather than compressional arc environments. According to previous studies (J. P. Encarnación et al., 1993; J. Encarnación et al., 1999; Geary et al., 1989; Yumul, 1996), the Coto block was generated ~1–2 Myrs before the Acoje block (44–43 Ma vs. 45 Ma), and the two blocks present geochemical affinities to back-arc and arc settings, respectively. However, systematic investigations show the two blocks are more likely different parts of the same oceanic fragment with transitional compositions (Geary et al., 1989). Although the Zambales blocks were dated to be formed at middle Eocene (46–44 Ma), they were possibly developed in the context of pre-Eocene lithospheres according to tectonic configuration (Perez et al., 2018; Wu et al., 2016), which can also be partly supported by the observation that the ophiolite is spatially bounded by a Western Mesozoic ophiolite belt and an Eastern Mesozoic-Eocene ophiolite belt (Queaño et al., 2017).

The crustal rocks in the Coto block display chemical variation from MORB-like to island arc tholeiitic (IAT) compositions continuously in a short time interval (J. Encarnación et al., 1999; Geary et al., 1989), and all these rocks were generated during development of the ophiolitic block itself rather than being captured from pre-Eocene

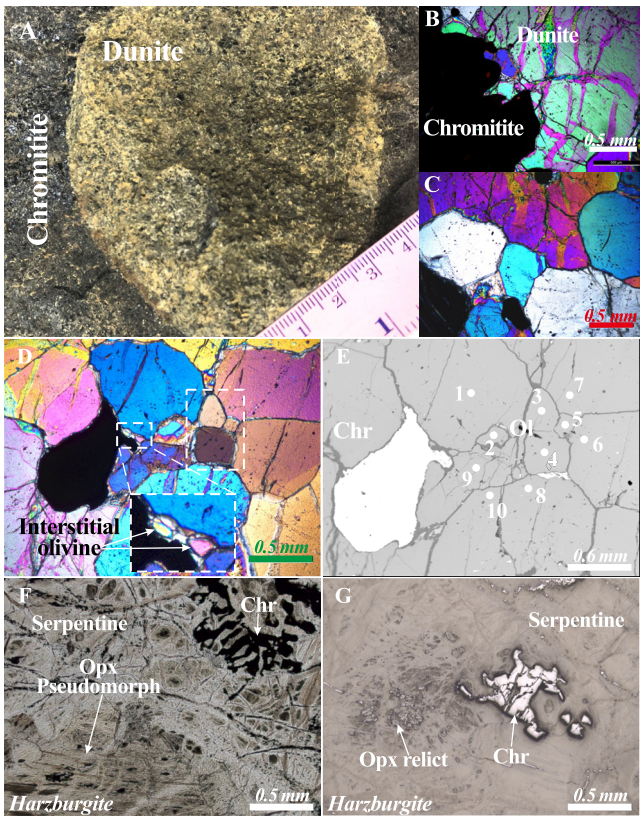

Figure 2. Petrographic features of chromitites, dunites and harzburgites. (a): Photo of the massive chromitite DEC-02 and its hosted dunite enclave. (b): Photomicrograph showing the dunite-chromitite border in the diagram (a). (c–e): Photomicrographs of the dunite enclave. The diagram (d) and (e) were taken for the same position using microscope and SEM, respectively. The boxes in the diagram (d) are used to mark the olivine grains (either euhedral and anhedral) that were most likely crystallized from trapped melts, based on their different interference colors from surrounding large grains The Fo values of spot 1–10 shown in the diagram (e) are analyzed to be 93.9, 94.2, 94.0, 94.2, 94.1, 93.8, 94.1, 94.1, 94.6, and 94.0, respectively, overall indistinguishable to each other with errors. Details of the data can be found in Table S4. (f–g): Photomicrographs of serpentinized harzburgites with chromite and orthopyroxene relicts.

ocean lithospheres. Especially, the MORB-like rocks show subduction-related features, for example, Nb-Ta negative anomalies in spider diagram, indicating that they were generated at a spreading center with a slab below rather than at a typical MOR setting (Yu, 2015). By contrast, volcanic rocks in the adjacent younger Acoje block are mainly made of IAT and boninitic lavas at the lower and upper lava sequences, respectively, with boninites occurring as pillow lavas at the topmost sequence (Perez et al., 2018). Compared with the magmatism developed at different spreading settings (e.g., MOR, back-arc basin, and proto-forearc), such rapid continuous compositional variation of magmas in the Zambales ophiolite is best explained as the result of evolving magmatism in a proto-forearc setting (Geary et al., 1989; Perez et al., 2018), consistent with the evolution trends of magmatism developed in the classical Troodos ophiolite, Oman ophiolite and the infant IBM arc (Whattam & Stern, 2011).

The Coto block consists stratigraphically of an upper mantle sequence, an MTZ, a cumulate troctolite-gabbro unit, and a volcanic-hypabyssal suite (Figure 1c; Geary et al., 1989; Leblanc & Violette, 1983). The upper mantle sequence mainly comprises harzburgites with porphyroclastic textures (Figures 2f–2g). The MTZ is generally ~200–300 m thick but some parts are as thin as <50 m (Figure 1c; Leblanc & Violette, 1983; Yumul, 2004). This zone is composed of serpentinized dunites and host chromitite pods. The chromitites exhibit disseminated to massive textures. With the modal % variation of chromite, disseminated chromitites change into massive ores (>80 modal % Chr) and dunites (<20 modal % Chr). From the MTZ dunites upward, there is a thin layer of Cpx/Pl-bearing dunites, marking the transition to the overlying troctolite-gabbro unit (Leblanc & Violette, 1983). The volcanic-hypabyssal suite marks the top sequence of the block and records a crystallization sequence of olivine + chromite → plagioclase → clinopyroxene → orthopyroxene (Yumul, 2004), consistent with that developed in SSZ ophiolites.

3. Petrography and Sampling

Chromitites in the Coto block are made up of mainly chromite and serpentine in varying proportions. Harzburgites and dunites have been highly serpentinized. Apart from some orthopyroxene relicts, few fresh olivine and orthopyroxene grains can be observed in the harzburgites (Figures 2f–2g). By contrast, chromite grains in the serpentinized harzburgites and dunites are well preserved and have either irregular (e.g., wormy) or subhedral shapes (Figures 2f–2g). The harzburgites and dunites contain ~1–8 modal % and 1–20 modal % chromite, respectively. The sizes of these chromite grains range from tens to hundreds of μm (Figures 2d–2f). The fresh dunite enclaves hosted in massive chromitites are made up of olivine grains of varying sizes (tens of μm to 3–4 mm) together with ~3 modal % subhedral to euhedral chromite (Figures 2c and 2d). Large olivine grains in the dunite enclaves have irregular shapes (Figure 2b), whereas small grains are euhedral to anhedral and occur as interstitial grains (Figures 2c and 2d).

We selected six harzburgites, eight dunites, and six chromitites from the open pit that is located at the border of the narrow MTZ and mantle sequence of the block (Figure 1c and Table 1). In particular, two dunite enclaves are selected and named as DE-01 and DE-02, respectively, and their massive chromitite hosts are accordingly named DEC-01 and DEC-02 (Table 1). In addition, four chromitite samples that were initially reported in Zhou et al. (2000, 2014) are also included in this study (Table 1).

4. Analytical Methods

The major oxide compositions of olivine and chromite were obtained with a JEOL JXA-8230 electron probe microanalyzer (EPMA) with a combined WDS/EDS system in the Department of Earth Sciences, the University

Journal of Geophysical Research: Solid Earth

10.1029/2022JB025562

Table 1
Averaged Major Element Compositions (wt.%) of Chromite in the Coto Harzburgites, Dunites and Chromitites by EPMA

Sample	H12	H16	H19	H20	H21	H22	D01	D02	D05	D06	D08	D09	D10	D11	DEC 01	DEC02	C26	C31	ZB07	ZB10	ZB03	ZB08	ZB12	ZB14
SiO_2	0.02	0.01	0.01	0.03	0.01	0.01	0.02	0.03	0.02	0.03	0.03	0.01	0.02	–	0.02	0.01	0.01	–	0.01	0.03	0.10	0.07	0.11	0.08
TiO_2	–	0.03	0.01	0.02	0.03	0.02	0.12	0.17	0.27	0.20	0.26	0.21	0.22	0.13	0.03	0.05	0.06	0.07	0.08	0.14	0.22	0.08	0.05	0.18
Al_2O_3	22.8	25.1	22.1	25.7	23.8	25.8	37.3	32.0	35.2	31.3	33.1	32.0	27.0	30.4	28.9	29.2	29.2	29.6	26.4	31.5	28.4	27.7	30.6	33.4
V_2O_3	0.23	0.18	0.22	0.24	0.23	0.2	0.14	0.16	0.13	0.15	0.15	0.16	0.16	0.17	0.16	0.16	0.17	0.17	0.17	0.13	–	–	–	–
Cr_2O_3	45.0	43.4	44.1	41.5	42.8	40.3	29.4	34.2	30.0	34.6	32.3	34.5	38.4	35.5	38.8	38.8	38.9	38.4	40.8	35.0	39.6	40.4	38.4	35.4
FeO	18.5	17.0	19.3	18.2	18.3	19.1	15.8	18.2	17.0	18.7	17.2	18.4	19.2	16.9	13.0	12.8	13	13.3	14.0	14.5	14.9	14.9	13.1	13.6
MnO	0.23	0.19	0.28	0.22	0.21	0.21	0.18	0.25	0.19	0.22	0.21	0.24	0.27	0.23	0.17	0.16	0.15	0.17	0.16	0.16	0.14	0.14	0.11	0.13
MgO	12.6	14.4	11.9	12.9	13.1	12.4	16.9	14.7	15.7	14.7	15.0	14.8	13.4	15.0	17.2	17.1	17.3	17.3	16.5	16.6	16.3	16.3	17.2	16.7
ZnO	0.19	0.11	0.16	0.11	0.09	0.24	0.07	0.12	0.11	0.17	0.11	0.15	0.14	0.06	0.06	0.02	0.05	0.04	0.03	0.02	–	–	–	–
NiO	0.05	0.07	0.07	0.09	0.10	0.07	0.15	0.16	0.15	0.12	0.14	0.13	0.11	0.16	0.2	0.21	0.22	0.2	0.15	0.21	–	–	–	–
Total	99.6	100.6	98.2	99.0	98.6	98.3	100.1	100.0	98.8	100.3	98.5	100.6	99.0	98.6	98.4	98.4	99.1	99.3	98.3	98.4	99.6	99.6	99.4	99.5
Cr#	57.0	53.7	57.2	52.1	54.8	51.2	34.6	41.7	36.4	42.6	39.5	42.0	48.8	43.9	47.4	47.2	47.3	46.6	51.0	42.7	48.3	49.5	45.7	41.6
Mg#	58.5	64.9	56.6	59.3	60.7	58.0	71.8	64.7	68.0	64.7	66.0	64.8	61.1	66.9	76.2	75.77	76.42	76.17	74.39	73.14	71.15	71.86	74.33	71.72
$Fe^{3+}/\sum Fe$	0.14	0.19	0.16	0.13	0.17	0.16	0.25	0.21	0.23	0.23	0.20	0.22	0.21	0.22	0.26	0.24	0.26	0.27	0.27	0.25	0.21	0.23	0.19	0.13
$TiO_{2\text{-Melt}}$															0.18	0.23	0.28	0.30	0.33	0.46	0.60	0.32	0.46	0.53

Note. (1) The difference between dunites and chromitites in this study is defined by the modal % of chromite, <20 modal % and >20 modal %, respectively, but chromitites used in this study are all massive chromitites with over 80 modal % chromite. (2) $TiO_{2\text{-}Melt}$: the TiO_2 contents of the parental magmas of the high-Al chromitites. The equations can be found in the Part 6.1 and Figure 6. (4) The data of ZB-03, 08, 12 and 14 are from Zhou et al. (2014). (4) The whole data set is listed in the Table S1.

of Hong Kong. The measurements were at 15 kV accelerating voltage, 20 nA beam current and 1 μm spot diameter. The counting duration varied from 10 to 30 s for most elements, but Ti in chromite was measured for 120 s. Natural and synthetic oxides were used as standards. The data were calibrated using the PAP matrix correction and ZAF procedure-based program. The analytical precisions for oxides >1.00 wt.% are below 1%. The precisions for TiO_2 in chromite are <5% when the TiO_2 contents are >0.10 wt.% and <10% when the TiO_2 contents are 0.01–0.10 wt.%. Given that the TiO_2 contents of our chromite grains are all <0.3 wt.% (Table 1 and Table S1), the precisions of our TiO_2 measurement have a maximum 2se uncertainty <0.03 wt.%. The $Fe^{3+}/\Sigma Fe$ ratios of chromite were calculated based on the ideal stoichiometry of spinel.

The Li isotopic compositions of olivine from the dunite enclaves were obtained using a CAMECA IMS1280-HR SIMS at the Institute of Geology and Geophysics, Chinese Academy of Sciences following the method of B. X. Su et al. (2015, 2016, 2020). For convenience and efficiency of analysis, olivine separates (rather than intact grains) broken from the dunite enclaves were caste in an epoxy resin. The mount was then polished, cleaned with deionized water and ethanol, and dried within an oven before being coated with pure gold. A primary O^- beam of 15–30 nA was accelerated at-13 kV onto the sample surface with an ellipsoidal beam size of about 20 μm × 30 μm. The instrument was tuned with energy slit width of 40 eV to achieve a mass resolution of 1,500. Positive secondary ions ($^6Li^+$ and $^7Li^+$) were collected with an ion multiplier in pulse counting mode. The counting time for ^6Li, 6.5 mass (background), and ^7Li in each cycle were 12, 4, and 4 s, respectively. Before each analysis, 180-s pre-sputtering was used without raster, and secondary ion beams were automatically centered in the contrast aperture and field aperture to ensure the secondary ion transmission. Each analysis consisted of 30 cycles and takes ~14 min. The Li isotopic composition is given as δ^7Li ($[(^7Li/^6Li)_{sample}/(^7Li/^6Li)_{standard} - 1] \times 1000$), in which the standard refers to the NIST SRM 8545 (L-SVEC; $^7Li/^6Li = 12.0192$). Two intra-lab olivine reference materials, 06JY31OL (Mg#[$100 \times Mg^{2+}/(Mg^{2+} + Fe^{2+})$], 90.3; Li, 2.7 ± 0.6 ppm; δ^7Li, +4.51 ± 0.33‰) and 06JY34OL (Mg#, 91.5; Li, 1.46 ± 0.08 ppm; δ^7Li, +3.33 ± 0.16‰), developed by B. X. Su et al. (2015), were used to calibrate the instrumental mass fractionation (IMF) and Li concentration. The IMF values calculated against the 06JY34OL and 06JY31OL during the analysis were 13.93 ± 0.97‰ and 14.66 ± 1.55‰ (2SD), respectively (Figure S1 in Supporting Information S1 and Table S2), consistent with each other within analytical uncertainties. The δ^7Li values of the olivine separates were calibrated with the IMF value obtained for the 06JY34OL. The Li concentrations in olivine were calculated based on their $^7Li^+$ count rates (cps/nA) relative to that of the 06JY34OL (1.46 ± 0.06 ppm, 2SD, B. X. Su et al., 2015). This calibration factor was applied to the 06JY31OL, yielding 2.17 ± 0.07 ppm and matching the reference value (2.7 ± 0.6 ppm, B. X. Su et al., 2015) within analytical uncertainties. The internal errors of δ^7Li are mostly better than 2.0‰ (2se) during analysis and detection limit of Li concentration less than 1 ppb. To overcome matrix effects, the calibrated δ^7Li values were further corrected with the equation $\delta^7Li_{real} = \delta^7Li_{analysis} + (Mg\#_{sample} - Mg\#_{reference\ material})$, based on the discovery that the δ^7Li value measured by SIMS decreases by ~+1‰ for each molar % increase of forsterite in olivine (B. X. Su et al., 2015).

5. Results

5.1. Chromite

Chromite grains in the peridotites and chromitites have large variations of Mg# and Cr# (Table 1 and Table S1). Those in the chromitites have Mg# and Cr# ranging from ~68 to 77 and ~42 to 51, respectively, falling in the range of N-MORB (Figure 3a). Chromite grains in the harzburgites have Mg# and Cr# ranging from ~54 to 67 and ~50 to 58, respectively, falling in the transitional area between abyssal and forearc peridotites (Figure 3a). The TiO_2 content of chromite increases from the harzburgites to dunites and chromitites, and those in the harzburgites have TiO_2 contents <0.1 wt.% (Figure 3b). Chromite grains in the dunites and chromitites have similar TiO_2 contents, 0.12–0.27 wt.% and 0.03–0.22 wt.%, respectively (Table 1 and Table S1). Such TiO_2 ranges are lower than that of chromite in MORB (usually >0.6 wt.%) but overlap that of chromite in boninites (<0.4 wt.%) (Figures 3b and 3c).

5.2. Olivine

Olivine separates from the dunite enclaves have Fo[$100 \times Mg^{2+}/(Mg^{2+} + Fe^{2+})$] values ranging from 92 to 95 (Table S3; Figures 4a and 4b), consistent with those values reported in Payot et al. (2013). These separates

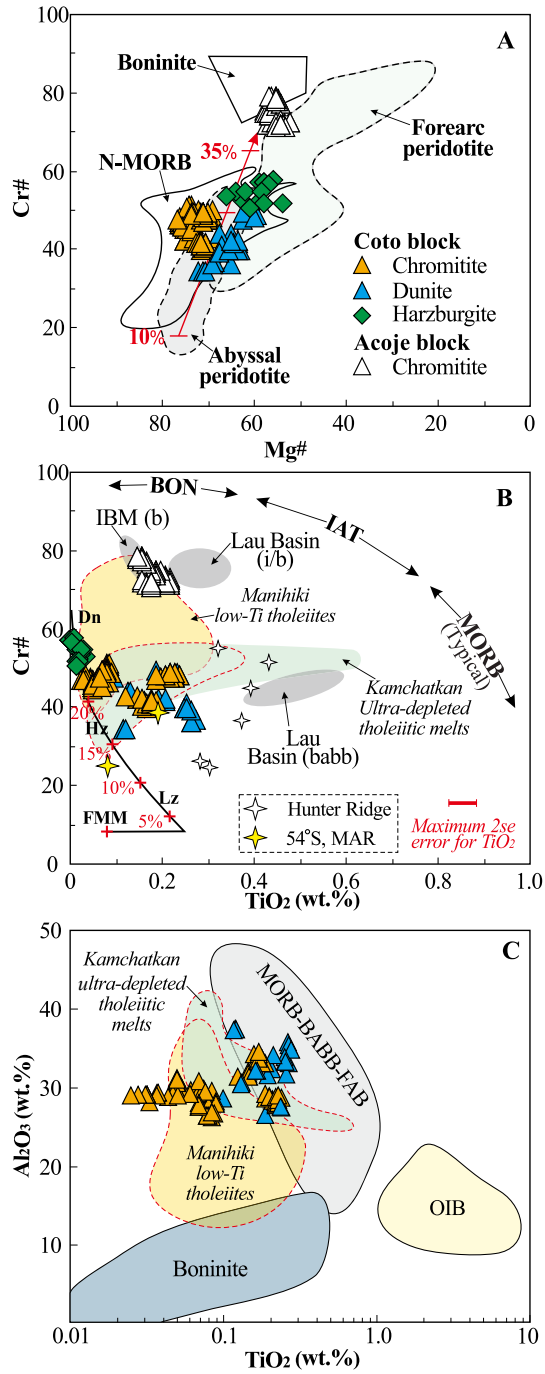

Figure 3. Compositions of chromite in the harzburgites, dunites and chromitites. (a): Plot of Cr# versus Mg# modified after Dubois-Côté et al. (2005). (b): Plot of Cr# versus TiO_2 modified after Pearce et al. (2000). The full names of abbreviations are as follows: Dn, dunite; FMM, fertile MORB mantle; Hz, harzburgite; Lz, lherzolite; b/BON, boninite; i/IAT, island arc tholeiite; MORB, mid-ocean ridge basalt; babb, back-arc basin basalt; FAB, forearc basalt; IBM, Izu-Bonin-Mariana. The data and ranges of chromite from the low-Ti tholeiitic lavas/melts of the Kamchatkan ophiolite (Far East), Manihiki Plateau (SW Pacific), Hunter Ridge (SW Pacific) and 54°S MAR basalts are from Portnyagin et al. (2009), Golowin et al. (2017), I. A. Sigurdsson et al. (1993) and Kamenetsky et al. (2001), respectively. Most chromite grains in the Kamchatkan low-Ti tholeiites have $TiO_2 < 0.35$ wt.%, as shown by the dashed red line in the diagram. The data of the Acoje high-Cr chromitites (white triangle) from Zhou et al. (2014) are also plotted in the diagram (a) and (b) for comparison. (c): Plot of Al_2O_3 versus TiO_2 modified after Golowin et al. (2017). The gray area marks the range of chromite from MORB-like lavas formed at spreading centers, all of which were simply classified as MORB in Kamenetsky et al. (2001) but clarified in this study to be the combination of typical MORB, BBAB and FAB.

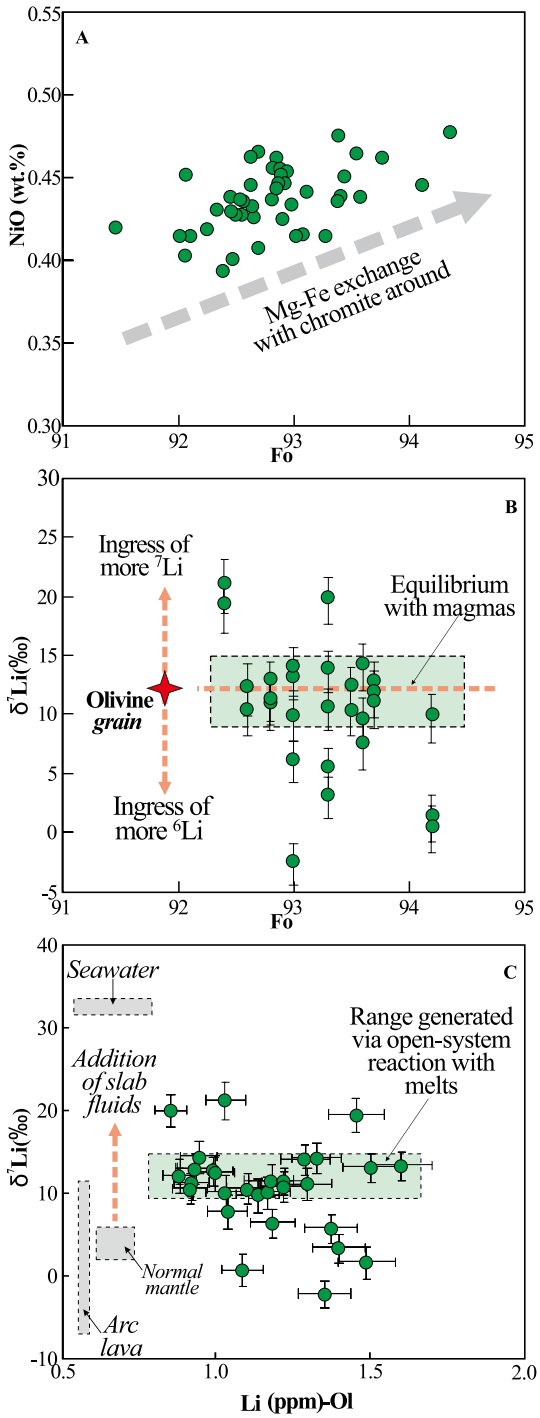

Figure 4. Compositions of olivine separates from the dunite enclaves. (a): Plot of NiO versus Fo. (b): Plot of δ^7Li versus Fo. The 2SD values of the reference material 06JY34OL (0.97‰) are considered in the error bars due to the effects of error propagation.

show increasing NiO content with increasing Fo value (Figure 4a). Their Li concentrations and δ^7Li values vary from 0.84 to 1.60 ppm and from −2.3‰ to +21.1‰, respectively (Table 2; Figures 4b and 4c). Generally, most of the olivine separates have little δ^7Li variation from their cores to rims, mainly between +10‰ and +15‰, but the δ^7Li values of a few analytical spots deviate to either higher or lower values, for example, up to +21.1‰ and down to −2.3‰ (Figures 4c and 5). The δ^7Li variation in some individual grain reaches 16‰ (Figure 5). In spite of the Li and δ^7Li variations, no systematic δ^7Li-Li correlation is observed (Figure 4c).

6. Discussion

6.1. Magmatic Origin of Low-Ti Chromitites in Ophiolites

Chromitites in ophiolites have been traditionally thought to be generated via massive precipitation of chromite in magma chambers (cumulate origin) or melt-peridotite reaction under high melt/rock ratio conditions in melt channels (replacive origin). In the latter case, the parental magmas of chromitites would react with peridotites on the melt channels and form dunite rims that surround chromitites, making up the podiform outlines of chromite deposits (Figure S2 in Supporting Information S1; Zhou et al., 1994). However, chromite grain in some high-Al chromitites in the Coto deposit have compositions similar to those chromite in harzburgites (Figure 3b). In particular, the data of chromite from some chromitites fall near the melting-trend line in the Cr# versus TiO_2 diagram defined by Pearce et al. (2000) (Figure 3b), seeming to suggest that these chromitites have residual origins. Cr is a compatible element in the mantle, and its concentrations in peridotites and mantle-derived melts increase with increasing degree of melting (Liang & Elthon, 1990). Due to the limited Cr concentrations of mantle peridotites, however, experimental works repetitively demonstrated that partial melting alone cannot even make chromite as the main phase of peridotites (Hirose & Kawamoto, 1995; Klingenberg & Kushiro, 1996; Matsukage & Kubo, 2003), not to mention converting peridotites to massive chromitites. Consequently, the possibility that chromitites could be formed via partial melting can be ruled out, and the low-Ti features of chromite in chromitites should therefore be attributed to other processes rather than partial melting.

Ophiolitic peridotites and mantle-derived magmas generally have <4,000 ppm Cr (<1,000 ppm for most MORB, up to 1,000–2,000 ppm for some boninites; H. Sigurdsson & Schilling, 1976; Cameron et al., 1979; Marchesi et al., 2006; Reagan et al., 2010; Uysal et al., 2012), whereas the Cr_2O_3 contents of massive chromitites mostly reach 40–60 wt.% based on the compositions of chromite (Figure 6; Zhou et al., 2014). Using mass-balance calculations, it is found that production of each fraction (wt.%) of massive chromitites requires 100–400 fractions of magmas, and even formation of disseminated chromitites (>20 modal % Chr) requires the amounts of magmas as at least 20 times as those of the chromitites (Figure 6a). The results corroborate that chromitites were all formed in melt-dominated environments, wherever and however they were formed. Although the so-called replacive chromitites are traditionally thought to be converted from peridotites by melt modification, the melt/rock ratios required for their formation in melt channels reach up to tens to hundreds. Such high melt/rock ratio conditions could definitely generate the same chemical effects as in pure magma environments, for example, in magma chambers, where crystallization of enough chromite could be ensured with sufficient Cr supply. Accordingly, formation of all ophiolitic chromitites, in either magma chambers or melt channels, can be considered to be achieved via massive precipitation and accumulation of chromite from

Table 2
Li Concentrations and Isotopic Compositions of Olivine in the Dunites

Grain	Spot	Li (ppm)	2SE	δ^7Li (‰)	2SE
DE-01 (dunite enclave)					
G01 (Fo, 92.6)	01 (core)	1.10	0.07	10.48	1.56
	02 (rim)	0.99	0.06	12.40	1.88
G04 (Fo, 93.0)	01 (rim)	1.32	0.08	14.15	1.54
	02 (core)	1.16	0.07	10.03	1.59
	03 (rim)	1.60	0.10	13.24	1.42
G11 (Fo, 92.4)	01 (core)	1.03	0.06	21.13	1.93
	02 (rim)	1.45	0.09	19.38	1.77
G16-01 (Fo, 92.8)	01 (core)	1.22	0.08	11.32	1.34
	02 (rim)	1.50	0.09	13.06	1.42
G18 (Fo, 92.8)	01 (core)	1.29	0.08	11.04	1.69
	02 (rim)	1.18	0.07	11.41	1.63
G22 (Fo, 93.3)	01 (rim)	1.37	0.08	5.65	1.48
	02 (core)	1.21	0.08	10.70	1.47
	03 (rim)	1.28	0.08	13.98	1.45
DE-02 (dunite enclave)					
G01 (Fo, 93.5)	01 (core)	0.91	0.06	10.43	1.54
	02 (rim)	0.99	0.06	12.54	1.48
G09 (Fo, 93.7)	01 (rim)	0.92	0.06	11.20	1.70
	02 (core)	0.88	0.05	12.00	1.67
	03 (rim)	0.93	0.06	12.93	1.50
G10 (Fo, 93.0)	01 (core)	1.18	0.07	6.31	1.42
	02 (rim)	1.35	0.08	−2.32	1.41
G11 (Fo, 94.2)	01 (rim)	1.08	0.07	0.62	1.63
	02 (core)	1.48	0.09	1.54	1.65
	03 (rim)	1.03	0.06	10.03	1.75
G15 (Fo, 93.6)	01 (rim)	1.03	0.06	7.69	1.64
	02 (core)	0.94	0.06	14.32	1.66
	03 (rim)	1.13	0.07	9.69	1.75
G19 (Fo, 93.3)	01 (core)	0.85	0.05	19.92	1.64
	02 (rim)	1.39	0.09	3.32	1.46

Note. (1) The whole data set of the major element compositions of olivine can be found in the Table S3, and the grain NO, used for Li isotopic analysis can also be found in the Table S3. (2) The 2se errors of the intra-lab reference material 06JY34OL were also considered in those of our data above due to the effect of error propagation during calibration.

magmas, defining their cumulate origin in a broad sense. In particular, the Coto deposit is the largest high-Al chromite deposit in the world and located at the dunitic MTZ of the block (Figure 1c), where mantle-derived magmas once gathered into magma chambers. Thus, accumulation of chromite grains in magma chambers would be the most probable way of forming the massive chromitites (>80 modal % Chr).

Although all ophiolitic chromitites can be considered as cumulate products of magmas from the perspective of Cr provenance, three possibilities other than partial melting still need to be considered to explain the low-Ti feature of chromite in some chromitites, including (a) the parental magmas of chromitites originally had low Ti contents (*P*1); (b) the parental magmas originally had high Ti contents but were modified to be Ti-depleted ones during reaction with Ti-poor peridotites (*P*2); and (c) the compositions of chromite in chromitites were modified during subsolidus ionic exchange (*P*3). Generally, it is a common sense that subsolidus ionic exchange with adjacent olivine during cooling modifies the compositions of chromite in chromitites. For example, Mg^{2+} and Ni^{2+} prefer to diffuse from chromite to olivine, whereas Fe^{2+}, Mn^{2+} and Zn^{2+} diffuse from olivine into chromite (Ozawa, 1983; Arai, 1994; O'Reilly et al., 1997), resulting in the high Fo values of olivine grains in chromitites (Figure 4a). Compared to divalent elements, however, Cr^{3+}, Al^{3+} and Ti^{4+} are much less compatible in olivine than in chromite and cannot be notably affected by ionic exchange (Kamenetsky et al., 2001; Wang et al., 2021). As a result, it is better to attribute the low-Ti features of chromite in chromitites to magmatic processes (*P*1 and *P*2).

Due to the incompatibility of Ti, the TiO_2 contents of mantle-derived melts generally have distinctly higher TiO_2 contents than mantle peridotites (>0.1 vs. <0.1 wt.%; Kamenetsky et al., 2001; Marchesi et al., 2006; Uysal et al., 2012; Xiong et al., 2017). Therefore, in the case of generating replacive chromitites in melt channels, it is possible that reaction with peridotites could possibly lowered the TiO_2 contents of the reactant melts, which may subsequently impose low-Ti features on the crystallized chromite and account for their residual-like compositions. Based on the melt/rock ratios required for formation of chromitites, the TiO_2 contents of peridotite reactants are calculated to take up <0.005% of the whole reaction systems, and the value would be lowered to 0.001% if the generated chromitites are massive ones (Figure 6b). Such results mean that the effects of peridotites on the Ti contents of melts can be generally ignored during the formation of replacive chromitites in melt channels. As a result, the low-Ti features of chromite in chromitites that disguise them as melting residues are not typical hybrid products between reactant melts and peridotites either, but were mainly inherited from the melts, no matter how low the TiO_2 contents of the chromite grains are. Given that chromitites formed in magma chambers were not obviously affected by melt-peridotite reactions, the TiO_2 contents of chromite in all ophiolitic chromitites can be used for studying the nature of their parental magmas.

In the Cr#-TiO_2 diagram, some data of chromitites are plotted between those of harzburgites and dunites (Figure 3b). Although the data distribution seems to suggest chromitites and dunites are the intermediate and ultimate reaction products between harzburgites and melts, respectively, such an explanation is inconsistent with the fact that chromitites were formed under higher melt/rock ratio conditions than dunites, in which sufficient supply of Cr was ensured. Previous studies have well demonstrated that chromite grains in chromitite lens/pods have higher TiO_2 contents than their dunite rims (Figure S3 in Supporting Information S1; Zhou et al., 1996; B. Su et al., 2019). Given that all chromitites were formed under melt-dominated conditions, formation of each chromitite represents one independent process of magma accumulation. Accordingly, the abnormal pattern of

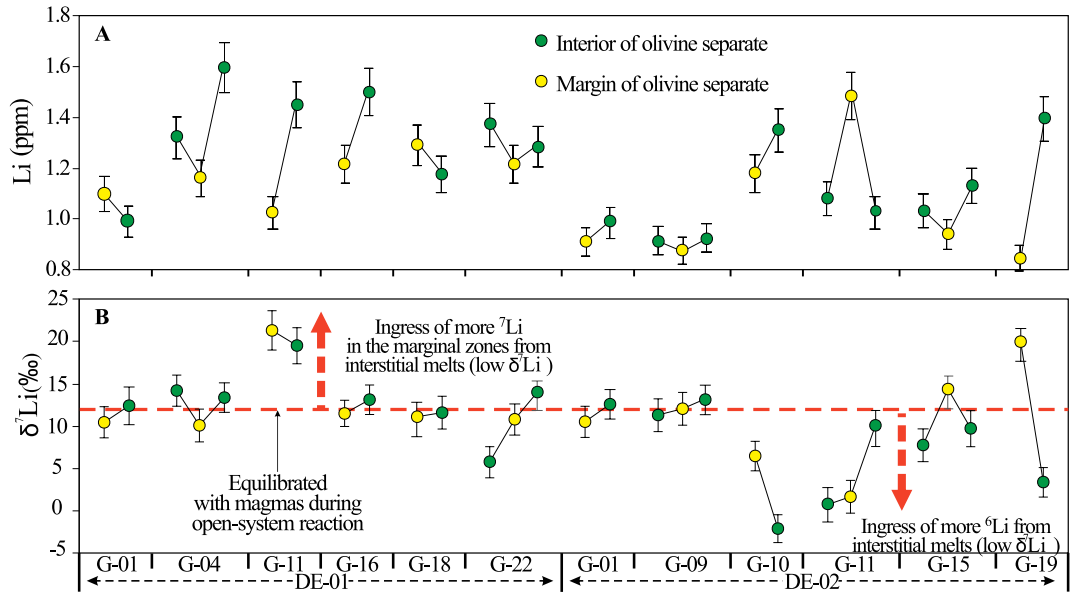

Figure 5. Variations of Li concentration and δ^{7}Li value in individual olivine separates from the dunite enclaves.

data distribution found in this study indicate that the dunites and chromitites were generated by multiple pulses of magmas rather than during one single event of fractional crystallization or melt-rock reaction, and linking all the chromitites and dunites with one trend arrow in the diagram would be misleading.

6.2. Parental Magmas and Mantle Sources of the High-Al Chromitites

Chromite grains in the high-Al chromitites have variable Cr#s and TiO_2 contents (Figures 3a–3c), indicative of varying compositions of their parental magmas. Such results are in agreement with the postulation that chromitites in the deposit were generated by multiple pulses of magmas. According to Kamenetsky et al. (2001), the TiO_2 contents of melt inclusions in chromite are well correlated with those of their chromite hosts (Figure 7), suggesting that the TiO_2 contents of chromite can be effectively used to estimate those of their parental magmas. Based on previous studies (Kamenetsky et al., 2001; Rollinson, 2008), two empirical equations have been derived to calculate the TiO_2 contents of parental magmas of chromitites:

$$TiO_2\,(\text{Melt}) = 1.5907 * [TiO_2\,(\text{Chr})]^{0.6322} \quad (\text{for high-Al chromite})$$

$$TiO_2\,(\text{Melt}) = 1.0963 * [TiO_2\,(\text{Chr})]^{0.7863} \quad (\text{for high-Cr chromite})$$

The calculated results show that the parental magmas of the Coto high-Al chromitites have a wide range of TiO_2 from 0.15 wt.% to 0.63 wt.% (Figure 7), overall lower than the TiO_2 ranges of typical MORB-like lavas (~0.6–1.7 wt.%; Ishizuka et al., 2020; Kamenetsky et al., 2001; Reagan et al., 2010; Shervais et al., 2019). This implies that the high-Al chromitites are not products of typical MORB-like magmas but those with more depleted compositions, for example, with low-Ti tholeiitic affinities (Figures 3b and 3c). Although such depleted lavas/melts were not reported in Kamenetsky et al. (2001), they were indeed found in the Kamchatkan ophiolite (Far East), Manihiki Plateau (SW Pacific), and Hunter Ridge (SW Pacific), and are associated with chromite with comparable compositions to the low-Ti chromite in our chromitites (Figures 3b, 3c, and 7; Portnyagin et al., 2009; Golowin et al., 2017; I. A. Sigurdsson et al., 1993), proving that there are indeed magmas in the world suitable for producing high-Al chromitites with low-Ti features. Particularly, the Hunter Ridge is the only contemporary example developed in the context of SI in the world (Patriat et al., 2019).

The compositions of mantle-derived magmas are controlled by the compositions of their mantle source, degrees of partial melting and extents of magma evolution (Green & Falloon, 2015; Klingenberg & Kushiro, 1996; Kushiro, 2001). The parental magmas of chromitites are magnesian enough to cumulate olivine and generate dunites (Arai, 1997; P. F. Zhang et al., 2016; Zhou et al., 1994, 1998). Such Mg-rich magmas are traditionally

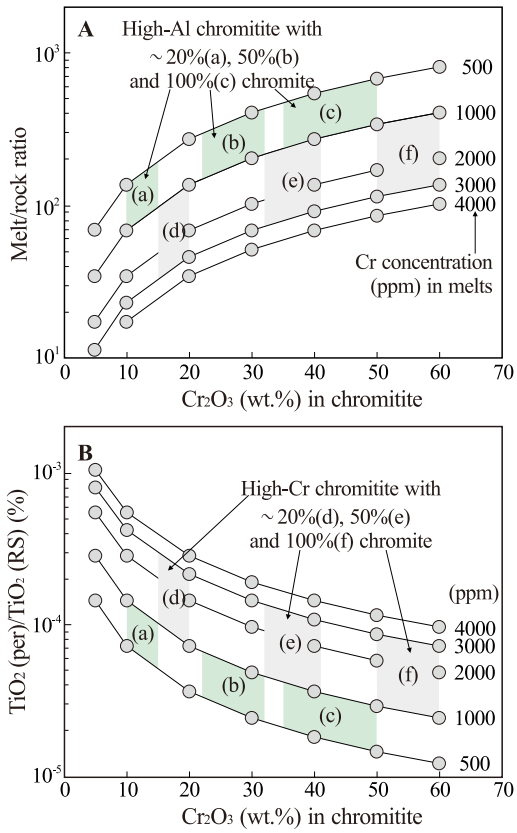

Figure 6. Contributions of reactant melts and peridotites to the formation of ophiolitic chromitites. (a): Mass balance calculations for melt/rock ratios required for formation of chromitites. Chromitites are assumed to only have chromite and olivine, the Fo and Mg# of which are set to be 93 and 70, respectively. The Cr# of chromite in the high-Al and high-Cr chromitites are assumed to range from 40 to 60 and 60 to 80, respectively. These representative values of chromite and olivine are selected based on the compositions of massive chromitites and their associated dunites worldwide (Zhou et al., 2014). The green and gray areas represent the general ranges for high-Al chromitites and high-Cr chromitites with varying vol.% chromite, respectively. Melts with 500–4,000 ppm Cr are used for the calculations. The parental magmas are commonly thought to have basaltic and boninitic compositions, which are assumed to have <1,000 and 2,000–3,000 ppm Cr, respectively. (b): Contributions of reactant peridotites (per) to the TiO_2 contents of the whole ore-forming reaction systems. Peridotites and mantle-derived melts generally have <0.1 wt.% and >0.1 wt.% TiO_2, respectively. For the convenience of calculations, the TiO_2 contents of both reactant peridotites and melts are assumed to be 0.1 wt.%, which would generate the upper limits for the contributions of reactant peridotites to the whole-system TiO_2.

thought to be primitive and unlikely to experience notable fractionation. As a result, the compositions of the parental magmas of chromitites are mainly controlled by those of their mantle sources and degrees of partial melting. Due to the incompatibility of Ti, lower degrees of melting of a common mantle source theoretically generate magmas with higher TiO_2 contents (Pearce et al., 2000). By contrast, Cr is a compatible element in the mantle, and its contents in mantle-derived magmas increase with increasing degrees of partial melting, for example, <300 ppm in MORB to up to 2,000 ppm in boninites (Cameron et al., 1979; Reagan et al., 2010). Assuming that the parental magmas of all ophiolitic chromitites were derived from similar mantle sources, the distinct behaviors of Ti and Cr imply that the TiO_2 contents of chromite in chromitites should decrease with increasing Cr#.

Although the TiO_2 contents of chromite in the high-Al chromitites are lower than those of chromite in MORB-like lavas at a certain Cr# (e.g., 45), they are comparable to, or even lower than, those of chromite in boninites and high-Cr chromitites (Figures 3b and 7). Such results indicate that the parental magmas of high-Al chromitites were derived from sources that were at least as depleted as those of boninitic lavas. According to the modeling of P. F. Zhang et al. (2020), 10% and 25% fractional melting of a fertile MORB mantle source would form melts with 1.28 wt.% and 0.71 wt.% TiO_2, respectively. By contrast, if the sources are residua after 10% and 15% fractional melting of fertile MORB mantle, with the melting degree increasing from 10% to 25%, the TiO_2 of melts generated from such depleted sources decreases from 0.45 wt.% to 0.23 wt.% and 0.23 wt.% to 0.11 wt.% respectively (Figure S4 in Supporting Information S1). Such calculated results also support that the parental magmas of high-Al chromitites were not originated from fertile MORB mantle but from already depleted sources. In addition, compared with melts derived from fertile MORB mantle, those generated from depleted sources (e.g., >10% melt depletion) at varying degrees of melting are inclined to have smaller TiO_2 variation (Figure S4 in Supporting Information S1)), explaining why chromite grains from high-Al and high-Cr chromitites have similar TiO_2 contents.

6.3. Origin of Olivine Grains in the Dunite Enclaves

Reaction between Mg-rich melt and peridotite is a prevalent feature of ophiolitic mantle sequences (Kelemen, 1990; Kelemen et al., 1992; Seyler et al., 2007; Zhou et al., 1994). The process dissolved pyroxene and precipitated olivine and chromite in peridotites, forming dunites and disseminated chromitites (Braun & Kelemen, 2002; Ghosh et al., 2014; P. F. Zhang et al., 2017, Q. Z. Zhang 2017). The dunite enclaves resulted from thorough pervasive reaction between harzburgites and parental magmas of the chromitite hosts (Mg-rich in compositions; Payot et al., 2013). With continuous crystallization and coating of chromite around the enclaves from magmas, those melts that infiltrated the enclaves would finally have been isolated by chromite grains (future chromitite hosts) and became trapped interstitial melts (Figure 8). Accordingly, the reaction in each enclave changed from an open to a closed system with time.

According to previous studies, trapped melts in mantle rocks occur either as thin films on crystal faces or melt pockets surrounded by minerals (Franz & Wirth, 1997; B. Su et al., 2010; Zhu et al., 2011). Although it is difficult to recognize the products of melt films, presence of fine-grained euhedral olivine aggregates among large irregular olivine indicates likely existence of melt pockets in the enclaves (Figure 2d). This is because such interstitial euhedral olivine grains show different interference colors from the surrounding ones, suggesting that they were unlikely broken from the latter ones. Moreover, such euhedral grains can best be explained as

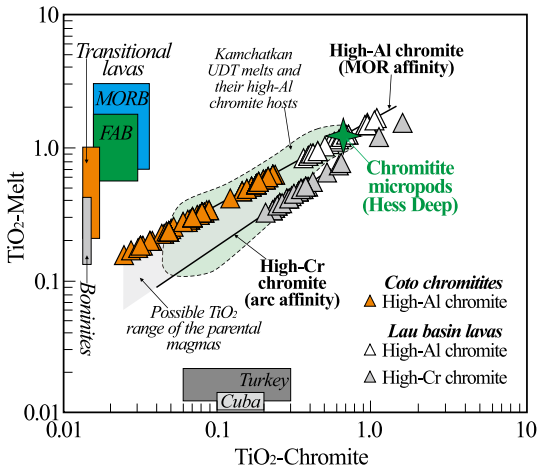

Figure 7. Calculated TiO_2 contents of the parental magmas of the high-Al chromitites. The empirical formula are from Rollinson (2008). The data of chromite from lavas of the Lau Basin and chromitite micropods of the Hess Deep are given for comparison, and they are from Allan (1994) and Arai and Matsukage (1998), respectively. The TiO_2 ranges of FAB, transitional FAB-boninitic lavas and boninites are plotted for comparison on the left side of the diagram based on the data shown in Reagan et al. (2010), Shervais et al. (2019), and Ishizuka et al. (2020). The TiO_2 range of MORB is from the PETDB geochemical database. The green area marks the range of high-Al chromite grains (Cr-rich spinel) and their hosted ultra-depleted tholeiitic melts from the Kamchatkan ophiolite. The parental magmas of the Coto chromitites may have even lower TiO_2 contents due to the subduction-related background, as shown in the gray area. The TiO_2 contents of chromite in high-Al chromitites from Turkey and Cuba are also shown at the bottom of the diagram for comparison, and the data are from Uysal et al. (2009) and González-Jiménez et al. (2011), respectively.

crystallization products of melt pockets that may allow unimpeded growth of crystals, accounting for their regular outlines. Although these interstitial olivine cannot be completely confirmed as products of melt pockets, it is noted that trapped melts must have existed in the enclaves as the result of melt infiltration, even if no supportive petrographic features are observed.

With the melt-harzburgite reaction, three types of olivine were generated in the dunite enclaves, including grains (a) previously existed in the harzburgite protolith but were modified by melts (Type-I; modified origin); (b) formed by replacement of pyroxene in the harzburgite protolith (Type-II; replacive origin); and (c) precipitating from trapped melts (Type-III; newly-crystallized origin). According to petrological observation and analysis, type-I and type-II grains cannot be distinguished from each other anymore, and even those grains possibly of the type-III origin show no major element difference from the former two types (Figure 2e). Such indistinguishable compositions of different olivine were possibly caused by thorough melt-rock reaction and fast Mg-Fe diffusion under mantle temperature conditions (Gordeychik et al., 2018; P. F. Zhang, Zhou, Liu, et al., 2019), which homogenized their major element compositions (in days based on experiments; Hirose & Kawamoto, 1995; Klingenberg & Kushiro, 1996).

6.4. Reaction and Diffusion-Induced Li Isotopic Variation in the Dunite Enclaves

The Li isotopic compositions of minerals can be easily affected by melt/fluid activities in rocks (Lai et al., 2015; Parkinson et al., 2007; Pogge von Strandmann et al., 2011; Rudnick & Ionov, 2007). Given the freshness of the dunite enclaves (Figures 2b–2e), the Li isotopic features of olivine grains in the dunite enclaves could not have been notably affected by serpentinization. Olivine grains in the enclaves experienced melt modification under early open and later closed system conditions, both of which may have largely influenced Li distribution in the olivine. As a result, the Li isotopic signatures of olivine in the dunite enclaves should have been mainly affected by processes related to the melt-rock reaction.

Olivine separates from the dunite enclaves mostly show no δ^7Li-Li correlation (Figure 4c), and the rims and cores of many single separates do not show identifiable Li isotopic difference (Figure 5b). Olivine grains in the enclaves were thoroughly modified by the infiltrating melts during the pervasive melt-harzburgite reactions. According to previous studies (Lundstrom et al., 2005; P. F. Zhang, Zhou, Robinson, et al., 2019), the Li isotopic compositions of olivine in dunites can be well buffered by melts under conditions of high melt/rock ratios and should be identical to those of the melts. Therefore, it is reasonable to assert that olivine grains in the enclaves were chemically equilibrated with the reactant melts during the open-system reaction, and that the no δ^7Li-Li correlation resulted from thorough modification by parental magmas of the high-Al chromitites, which should also have δ^7Li values ~+12‰ to +13‰ (Figures 4b–4c).

Although the analyzed olivine separates mostly have consistent Li isotopic compositions, some separates have large δ^7Li variations (up to +20‰), and their Li and δ^7Li values show no systematic co-variation from the interiors to the marginal zones (Figure 5b). Such features are unlikely to have been generated during the main episode of melt-peridotite reaction (open-system), but requires kinetic diffusion of Li that caused fractionation between ^{6}Li and ^{7}Li in the grains. As has been mentioned, the infiltrating melts in the dunite enclaves finally became isolated from the main magma body after the enclaves were coated by chromite. Once isolated in a closed system without replenishment from outside, the compositions of the trapped melts could not be maintained and would evolve with time. Because Li is incompatible in olivine and prefers to be retained in melts, the trapped melts must have developed increasingly higher Li concentrations with continuous solidification. Due to presence of concentration gradient, diffusion of Li theoretically took place from the trapped melts to surrounding olivine (Type-I and -II) under closed-system conditions (Figure 8).

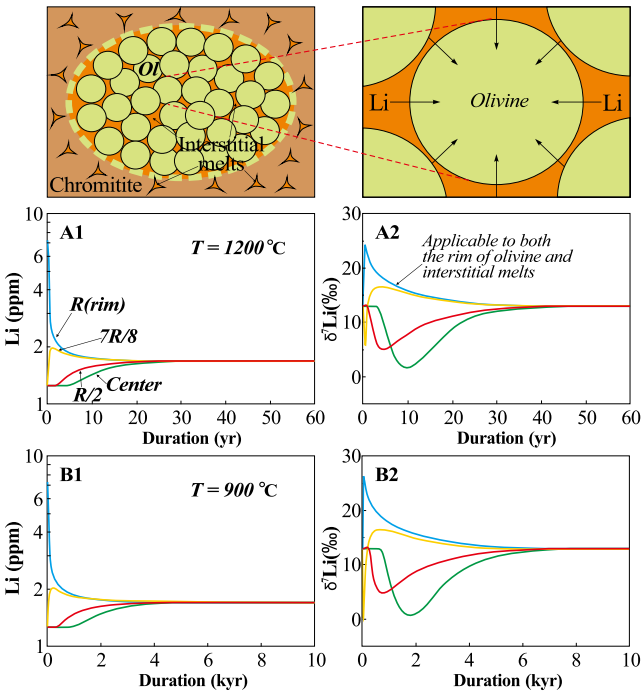

Figure 8. Modeling of Li ingress from trapped melts into olivine in the dunite enclaves under 1200 and 900°C, respectively. The dunite enclaves had been separated from the magma body by chromite grains during this stage. The Li concentrations and δ^7Li values at the rim, 7*R*/8, *R*/2 and center of the olivine core are shown with blue, yellow, red and green lines, respectively. More details can be found in the Part 6.4.

According to Parkinson et al. (2007), the δ^7Li values of olivine in peridotites can be modified in various ways during ingress of Li from trapped melts, quite different from the results generated during open-system reactions. On one hand, due to the faster diffusivity of ^{6}Li than ^{7}Li, diffusion of Li would transfer more ^{6}Li from the trapped melts into olivine, resulting in low-δ^7Li areas in the interiors of olivine grains. On the other hand, preferential loss of ^{6}Li from the trapped melts would cause higher and higher δ^7Li values of the melts, and the marginal zones of olivine grains would subsequently acquire higher δ^7Li values due to loss of more ^{6}Li to the grain interiors and ingress of more ^{7}Li from the trapped melts. As a result, the δ^7Li values of olivine grains can be meanwhile decreased in their interiors and elevated at their margins during ingress of Li from the trapped melts. This explains why some of the analyzed spots have δ^7Li values either higher or lower than the range generated during the open-system reaction (+10‰ to +15‰; Figures 4b–4c).

Based on the distribution and amounts of interstitial olivine grains (<5 vol.%), the volume of trapped melts in each dunite enclave should be much lower than that of the Type-I and Type-II olivine grains, and not all olivine grains were surrounded by trapped melts. This suggests that the closed-system diffusion of Li only affected a few grains, and many others, especially the inner parts of larger grains (e.g., 3–4 mm, Figures 2b–2d), were unlikely affected by the diffusion, so that their Li isotopic features obtained during the open-system reaction are well preserved, explaining why the δ^7Li values of most analytical spots fall into the narrow range (~+10‰ to +15‰; Figures 4b–4c). Moreover, because of the rapid diffusivity of Li, large Li isotopic variations in mantle rocks cannot survive for long under high temperature conditions (Gao et al., 2011; Halama et al., 2009; Lai et al., 2015; P. P. Liu et al., 2020; Marschall & Tang, 2020; Parkinson et al., 2007). Thus, the MTZ of the Coto block should have cooled fast so that the large δ^7Li variation of olivine in the dunite enclaves could be preserved.

6.5. Effects of Slab Input on the Mantle Sources of the Chromitites

The Li isotopic features of olivine separates from the dunite enclaves imply that the parental magmas of the high-Al chromitites had heavy Li isotopic compositions (average δ^7Li value, ~+12‰ to +13‰). Because Li isotopes cannot be remarkably fractionated during partial melting (Jeffcoate et al., 2007; Tomascak et al., 1999), mantle-derived melts theoretically have δ^7Li values identical to their mantle sources. According to previous studies, N-MORB and normal mantle regimes are thought to have a δ^7Li range of ~+4 ± 2‰ (Marschall et al., 2017; Tomascak et al., 2008), lower than the δ^7Li values of parental magmas of the high-Al chromitites (Figure 4c). Thus, the parental magmas of the high-Al chromitites could not have been produced from normal mantle regimes but from regions with heavier Li isotopic compositions.

Surficial materials, such as seawater and altered oceanic crustal rocks, generally have heavier Li isotopic compositions than normal mantle (Figure 4c; Chan et al., 1992, 2002; Marschall et al., 2007). Although the effects of slab components on the Li isotopic systems of sub-arc mantle vary among different subduction zones, as revealed by the δ^7Li values of arc lavas (~−7‰ to +12‰; Figure 4c; Agostini et al., 2008; Chan et al., 2002; Elliott et al., 2004; Moriguti & Nakamura, 1998; Tang et al., 2010; Tomascak et al., 2000, 2002), addition of slab-derived materials is the primary way of causing large-scale heavy Li isotopic anomalies in the mantle. Given that the Coto block is thought to have a SI origin and was generated in a proto-forearc setting (Geary et al., 1989; Perez et al., 2018; Yumul et al., 2020), the high-δ^7Li components required in the mantle sources of the high-Al chromitites can be reasonably attributed to slab components.

6.6. Numerical Constraints on the Closed-System Li Diffusion and MTZ Cooling

Usage of olivine separates for the analysis hinders our complete understanding of the whole diffusion processes of Li from the trapped melts to surrounding olivine, for example, the non-systematic δ^7Li-Li co-variation. In order to better comprehend how the large Li isotopic variations were generated in olivine grains, modeling is

needed to validate interpretations of the data. Moreover, the spreading rates of oceanic ridges are overall negatively correlated with cooling rates (Coogan et al., 2007). Although SI is accompanied by proto-forearc extension, but little work has been done on the transitional period between the FAB and boninitic magmatism. Given that Li isotopes are powerful speedometers for evaluating cooling rates of geologic processes, modeling the closed-system Li diffusion would also help to investigate the spreading rate and geothermal condition during the transitional FAB-boninitic magmatism.

To constrain the origin of the large Li isotopic variation of olivine and cooling rate of the thin MTZ beneath the Coto proto-forearc region, we carried out numerical modeling to recover the processes of closed-system and subsolidus Li redistribution in the enclaves by using a concentric spherical model. The inner core was assumed to be occupied by olivine that was equilibrated with the parental magmas of the high-Al chromitites. Because increase of Li concentrations in the trapped melts was driven by the solidification process, the outer shell was directly assumed to be occupied by olivine that had Li concentrations and isotopic compositions the same as the parental magmas of the high-Al chromitites, and its Fo value was fixed the same as that of the inner olivine in order to facilitate the modeling. The diffusion equation and some boundary conditions are listed below:

$$\frac{\partial C}{\partial t} = D(T)\left(\frac{\partial^2 C}{\partial r^2} + \frac{2}{r}\frac{\partial C}{\partial r}\right) \tag{1}$$

$$\frac{\partial C}{\partial t} = 0, r = 0, r = \mathrm{E}, t > 0 \tag{2}$$

$$D(T)\frac{\partial C}{\partial r} = D(T)\frac{\partial C}{\partial r}, r = \mathrm{R}, t > 0 \tag{3}$$

where (a) the variable $D(T)$ is the temperature-dependent diffusion coefficient of Li in olivine and can be obtained by $log[D(T)] = -5.92 - 1.2847 \times 10^4/T$ (Dohmen et al., 2010). The differences of $D(T)$ between ^{6}Li and ^{7}Li are determined by $D_7/D_6 = (m_6/m_7)^{\beta}$, in which β is thought to be 0.27 (Richter et al., 2014). (b) The variable r and t refer to the distance to the center of the spherical system and diffusion duration, respectively. (c) The parameters R and E are the radii of the inner olivine and the exterior radius of the outer shell, respectively. (d) The Equation 2 describes no diffusion in the center and surface of the spherical system, and Equation 3 describes the conservation of flux of Li across the core-shell boundary during diffusion.

The Fo values of the two spheres were set as 93 and remain constant throughout the modeling. The density of the olivine can be calculated based on the proportions of the end members of forsterite (Fo) and fayalite (Fa) with formulas below:

$$\begin{gathered}\rho_{\mathrm{i}}(T) = \rho_{\mathrm{i}}^{o}(298.15\,\mathrm{K}) + a(T - 298.15\,\mathrm{K}) + b(T - 298.15\,\mathrm{K})^2 \\ \rho_{\mathrm{OI}}(T) = \Sigma X_{\mathrm{i}}\rho_{\mathrm{i}}(T)\end{gathered} \tag{4}$$

Equation 4 was used to calculate the temperature-dependent density ρ of forsterite and fayalite, and the overall density of olivine (the weighted average value); the variable X_i represents the mole fraction of forsterite and fayalite. The coefficients a and b are constant and can be found in Niu and Batiza (1991).

After thorough reaction with parental magmas of the high-Al chromitites under open-system conditions, the Li concentrations and δ^7Li values of olivine in the dunite enclaves became ~0.8–1.6 ppm and +10‰ to +15‰, respectively, whereas trapped melts in the dunite enclaves, occurring as thin films wrapping the olivine grains, theoretically still had Li and δ^7Li values similar to those of the parental magmas. The partition coefficient of Li between olivine and melts varies largely in different studies, for example, 0.1–0.2 in Brenan et al. (1998) and ~0.425 in Ottolini et al. (2009). Olivine grains in the dunite enclaves thus had ~0.8–1.6 ppm Li. For a general evaluation of the closed-system diffusion process, the inner core and outer shell were assumed to have 1.25 and 10 ppm Li, respectively, and their initial δ^7Li values were both set to be +13‰ based on the above information. Given the grain size of olivine in the enclaves, the radius of the inner core (R) was set to be 3 mm, and the thickness of the outer shell was set to be 0.03 mm, 1% of the radius of the inner core. The compositions and sizes of the inner core and outer shell are shown as below:

$$C = 1.25\,\mathrm{ppm}, \delta^7\mathrm{Li} = +13‰, r \le 3\,\mathrm{mm}, t = 0 \tag{5}$$

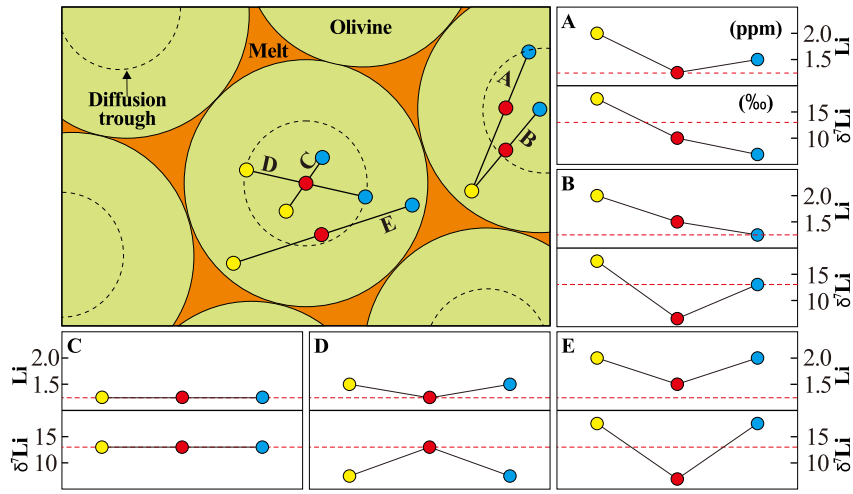

Figure 9. Expected varying δ^7Li-Li correlation patterns recorded by olivine separates from the dunite enclaves. The dashed circles are assumed to mark the diffusion trough that have the lowest δ^7Li values. Locations outside and inside the dashed circles have higher δ^7Li values than the diffusion trough. The marginal zones of the grains have the highest δ^7Li values according to the modeled results. The centers and zones nearby that were not affected by the ingress of Li are assumed to have 1.25 ppm Li and δ^7Li values of +13‰ (Diagram (c)). However, it is noted that the Li and δ^7Li values at other sites (e.g., the margins) in the olivine were assumed semi-quantitatively for reference based on the modeled results in Figure 8.

$$C = 10\,\text{ppm}, \delta^7\text{Li} = +13‰, 3\,\text{mm} \le r \le 3.03\,\text{mm}, t = 0 \quad (6)$$

Numerical modeling of the closed-system diffusion process was done using a finite element method programmed with Comsol Multiphysics. The isotopes ^{6}Li and ^{7}Li were taken as independent elements during modeling and processed separately under constant temperature conditions of 1200°C and 900°C, respectively (Figure 8). The first is generally comparable to the near-solidus temperature of mantle-derived melts, and the latter corresponds to the general temperature conditions in the MTZ below spreading centers (Boudier & Nicolas, 1995; Gao et al., 2011; McKenzie et al., 2005). The temporal variation of Li and δ^7Li values at the rim (R), 7R/8, R/2 and center of the inner olivine core were specially modeled for understanding the general diffusion processes of Li in the spherical system (Figure 8).

The results show that the inner part (e.g., center and R/2) of the olivine core shows decrease of δ^7Li with the increase of Li concentration, whereas the δ^7Li values of marginal zones (e.g., rim and 7R/8) increase at first and then fall back (Figure 8). Such results support that ingress of Li into olivine from trapped melts under closed-system conditions could meanwhile elevate and decrease the δ^7Li values in the grains (Figures 4c and 5b), consistent with the results of Parkinson et al. (2007). The highest and lowest δ^7Li values obtained by using in-situ analysis, −2‰ and +21‰, could be both reproduced by the modeling. It is noteworthy that the sizes of olivine grains and the amounts of trapped melts are variable at different locations in the real case of the dunite enclaves. Thus, it is suggested that olivine grains in the dunite enclaves record results of Li diffusion at different stages, and their Li isotopic compositions were modified to varying degrees during the close-system diffusion (Figure 8). Given that the olivine separates are broken pieces of large grains, it should be noted that they could be any parts (either marginal or inner zones) of the original olivine grains, explaining their various δ^7Li profiles and non-systematic δ^7Li-Li correlations (Figure 9).

Based on the modeled results, it takes <40 years to reach elemental and isotopic equilibrium in the spherical system under 1200°C (Figures 8a1 and 8a2). Given that the temperature during the main magmatic stage was likely even higher than 1200°C, the Li isotopic system of the whole enclaves could have been quickly homogenized during the open-system reaction, also supporting that the Li isotopic compositions of olivine can be easily buffered by melts under conditions of high melt/rock ratios. The results also show that it took ~6,000–8,000 years for Li to reach both elemental and isotopic equilibrium in the olivine separates at 900°C (Figures 8b1 and 8b2). However, a duration of 1,000–3,000 years is long enough to achieve the large Li isotopic variations detected in the olivine separates (Figures 8b1 and 8b2). Given that closed-system Li diffusion actually started under near solidus temperatures (~1200°C) and continued to subsolidus conditions, the time scale for generating large

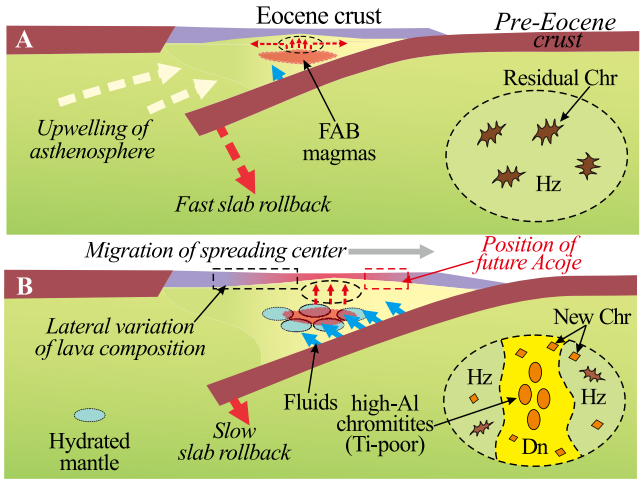

Figure 10. Diagrams showing the changing magmatism and mineralization of high-Al chromite in the Coto proto-forearc region during subduction initiation. (a): Partial melting in the fertile uppermost mantle in the context of slab rollback generated Eocene FAB in the context of Pre-Eocene oceanic lithospheres and harzburgitic mantle residue. Chromite grains in the residual harzburgites are featured by anhedral (e.g., wormy) shapes after partial melting. (b): Addition of slab-derived fluids took place in the mantle wedge and lowered the solidus temperature of the harzburgites, generating melts with lower TiO_2 contents than the FAB. Reaction between the low-Ti melts and harzburgites resulted in dunites and high-Al chromitites (TiO_2 of chromite < 0.35 wt.%). Because of melt infiltration during the high-Al chromite mineralization, euhedral chromite grains may appear in the harzburgites. It is noteworthy that the spreading center migrated during continuous slab rollback, and caused lateral variation of lava compositions in the crust, marked by color gradient from red (later) to purple (early). Details of the small circles below spreading centers can be found in the larger ones in each diagram.

Li isotopic variation in single olivine grains should be <1,000–3,000 years. Accordingly, the MTZ of the Coto block possibly cooled down at a minimum rate of ~0.1°C/yr. comparable to the MTZ and uppermost mantle below slow to ultra-slow spreading centers, for example, 0.3–5°C/yr for the Gakkel Ridge of the Arctic Ocean (P. P. Liu et al., 2020).

6.7. Geodynamic Implications for Subduction Initiation

The low-Ti features of chromite in the high-Al chromitites indicate depletion in the mantle sources of their parental magmas. Such pre-mineralization depletion can be possibly linked to MORB-like FAB magmatism in the Zambales ophiolite, which took place at the earliest stage of SI and just prior to the IAT formation. Further combining our petrological observations and geochemical data, a detailed evolutionary model can be reconstructed for the Coto proto-forearc region, specially from the perspective of mantle. First, the FAB was generated via decompressional melting of asthenosphere below the Zambales proto-forearc (Figure 10a). This left an harzburgitic mantle wedge and resulted in the irregular shapes and low TiO_2 contents of chromite in the harzburgites (Figures 2f–2g and 10a). Second, the depleted mantle wedge was hydrated by slab-derived fluids (Figure 10b). Such a process contributed to the heavy Li isotopic features in mantle sources of parental magmas of the high-Al chromitites and also accounted for the formation of subduction-related crustal rocks.

Although boninitic magmas are also the melting products of hydrous harzburgitic mantle, the Coto block has no record of boninitic magmatism. Such a fact implies that evolution of the Coto block itself did not cover the entire SI and expired after the transitional FAB-boninitic magmatism before boninites were formed. The compositions of mantle-derived magmas are controlled by both the compositions of their mantle sources and geothermal gradients. According to the calculated TiO_2 contents (Figure 7; Figure S4 in Supporting Information S1), the parental magma sources of both high-Al and high-Cr chromitites were harzburgitic and sometimes experienced similar degrees of melt depletion. Given that slab components are widely found in parental magma sources of high-Cr chromitites (Chen et al., 2019; P. F. Zhang, Zhou, Robinson, et al., 2019; P. F. Zhang et al., 2021), it is possible that the mantle sources of both types of chromitites often have similar compositions. Accordingly, absence of boninitic magmatism in the Coto block appear unrelated to mantle compositions, and production of transitional FAB-boninitic and boninitic lavas at the different stages of SI is better attributed to varying geothermal conditions rather than chemical variation of their mantle sources.

Numerical modeling show that the MTZ rocks of the Coto block cooled at a rate comparable to that observed for the uppermost mantle below ultra-slow to slow spreading centers, which extend at rates <20 and 20–50 mm/yr, respectively (Dick et al., 2003). Such a result indicates that mineralization of the high-Al chromite possibly occurred during a period when magmatic crustal spreading was not vigorous in the Zambales proto-forearc. According to the SI model, proto-forearc spreading is accompanied by asthenospheric upwelling, both processes driven by slab rollback (Reagan et al., 2010, 2019; Stern et al., 2012; Whattam & Stern, 2011). Thus, mineralization of high-Al chromite and related magmatism possibly mark a slow-motion period of slab rollback, which would not induce notable asthenospheric upwelling and subsequent proto-forearc spreading. This is not entirely consistent with the overall rapid spreading rates of proto-forearcs, for example, ~72 mm/yr on average for the IBM from the FAB to boninitic magmatism (Reagan et al., 2017, 2019), but suggests existence of sluggish intervals of slab rollback during SI.

Effective asthenospheric upwelling would be expected to induce high heat flow and ambient temperatures in overlying lithospheric mantle (He, 2014; Ueda et al., 2008). Previous studies revealed that both the FAB and boninitic magmatism were possibly developed under conditions >1400°C at 1–2 GPa (Falloon & Danyushevsky, 2000; Shervais et al., 2019), consistent with the effects of notable slab rollback and astheno-

spheric upwelling. By contrast, the low proto-forearc spreading rate during the high-Al chromite mineralization suggests that relevant magmatism took place under a comparatively low geothermal gradient, defining a trough period of heat flow in the whole process of SI. Such geothermal variation explains why the parental magmas of high-Al and high-Cr chromitites could be produced from similar mantle sources but at different stages of SI.

Based on the chemo-thermal variations discussed above, fluid-aided magmatism during the post-FAB period of SI may be divided into the early and late stages of flux melting, corresponding to productions of transitional FAB-boninitic (low-Ti IAT) and boninitic lavas, respectively. From the perspective of chromitites, the high-Al and high-Cr varieties result from the early and late stage of flux melting, respectively. Due to the lower geothermal gradients, the early stage of flux melting is probably marked by lower rates of magma production than the later stage. This is supported at least by the facts that: (a) high-Al chromite deposits are much rarer than high-Cr ones in the world; (b) reserve of the Coto deposit (6.34 Mt) is comparable only to that of an average high-Cr deposit (e.g., Luobusa deposit, average, ∼7 Mt, Q. Z. Zhang, Ba, et al., 2017; Kempirsai deposit, the largest, >310 Mt, Melcher et al., 1997).

According to previous studies, spreading centers in proto-forearcs move relative to trenches with on-going slab rollback, and lavas generated at spreading centers evolve from FAB to boninites, resulting in lateral variation of crustal compositions in proto-forearcs (Figure 10b; Dilek & Thy, 2009; Reagan et al., 2017, 2019). Comparing with the established model, the Coto and Acoje blocks were probably formed at different spreading stages of the Zambales proto-forearc, and continuous slab rollback caused migration of the spreading center from location of the Coto block to that of the younger Acoje block (Figure 10b). Accordingly, it is possible that the Coto block possibly became an off-axial region with few magmas further produced after the high-Al chromite mineralization, accounting for absence of boninites in the block.

Different from the Zambales ophiolite, development of proto-forearcs and SSZ ophiolites may not always follow the classical rule of SI (Stern et al., 2012; Whattam & Stern, 2011). Even in an individual ophiolite that consists of multiple blocks, the geological processes recorded in each block differ and may not be able to cover the whole evolutionary history of classical SI, for example, the case of Coto block. Moreover, in case that slab rollback is slow without notable upwelling of asthenosphere at the very beginning of SI, slab dehydration would probably prevail. Such a geodynamic setting would hinder the generation of FAB but facilitate flux melting in advance, producing IAT of both high-Ti (early) and low-Ti (later) varieties and boninitic magmas with the on-going slab rollback and depletion of magma sources. Obviously, the high-Ti and low-Ti IAT generated in the case above can be overall considered as the counterparts of FAB and transitional FAB-boninitic lavas that formed in classical model of SI, respectively. Alternatively, if true subduction of slabs happens at the beginning of SI with no slab rollback taking place from then on, subduction zones would directly take shape and be followed by crustal uplifting and arc magmatism that usually varies from IAT to calc-alkaline ones with time (the case of induced SI; Stern, 2004). In this case, neither FAB or boninitic lava is likely to be produced, and the required spreading setting for origin of ophiolites cannot be satisfied either.

7. Conclusions

1. Parental magmas of the high-Al chromitites of the Coto block had transitional FAB-boninitic compositions, and their mantle sources were harzburgitic and modified by slab fluids, accounting for the low TiO_2 contents of chromite and heavy Li isotopic signatures of olivine in the Coto chromite deposit.
2. The large δ^7Li variation of olivine grains in the dunite enclaves was caused by ingress of Li from interstitial melts under closed-system conditions. A minimum cooling rate of 0.1°C/yr was required in the MTZ of the Coto proto-forearc region in order to preserve the observed isotopic variation.
3. The transitional FAB-boninitic magmatism took place in the early stage of flux melting during SI. This possibly marked a trough in heat flow and magma production during the entire course of SI, as the result of slow slab rollback and accompanied asthenospheric upwelling then.
4. Development of magmatism in the Coto proto-forearc region expired soon after the transitional FAB-boninitic magmatism. This was possibly due to migration of spreading center to the adjacent Acoje region, accounting for the week magmatism in the Coto block after the high-Al chromite mineralization.

Data Availability Statement

The compositional data used in this study can be found in the repository of "Figshare" via https://doi.org/10.6084/m9.figshare.22147448.v1.

Acknowledgments
This study is supported by the National Natural Science Foundation of China (42172074 and 91962217), the Fundamental Research Funds for the Central Universities (CUG2106105), and the Collaborative Research Grant from the Key Laboratory of Mineralogy and Metallogeny, Guangzhou Institute of Geochemistry, Chinese Academy of Sciences (KLMM20190201). Many thanks to Nikko Pacle and Americus Perez for their great assistance during the field excursion. We are also grateful to Prof. Paul Robinson, Prof. Ibrahim Uysal, Dr. Brain O'Driscoll for their beneficial discussions and suggestions during the revision. The constructive comments and suggestions from the editors, Prof. Paul Tomascak, Prof. Tomo Morishita and two other anonymous reviewers are highly appreciated.

References

Agostini, S., Ryan, J. G., Tonarini, S., & Innocenti, F. (2008). Drying and dying of a subducted slab: Coupled Li and B isotope variations in Western Anatolia Cenozoic Volcanism. *Earth and Planetary Science Letters*, *272*(1–2), 139–147. https://doi.org/10.1016/j.epsl.2008.04.032

Allan, J. F. (1994). Cr-spinel in depleted basalts from the Lau basin backarc: Petrogenetic history from Mg-Fe crystal-liquid exchange. In *Proceedings of the ocean drilling program. Scientific results* (Vol. 135, pp. 565–583).

Arai, S. (1994). Characterization of spinel peridotites by olivine-spinel compositional relationships: Review and interpretation. *Chemical Geology*, *113*(3–4), 191–204. https://doi.org/10.1016/0009-2541(94)90066-3

Arai, S. (1997). Origin of podiform chromitites. *Journal of Asian Earth Sciences*, *15*(2–3), 303–310. https://doi.org/10.1016/s0743-9547(97)00015-9

Arai, S., & Matsukage, K. (1998). Petrology of a chromitite micropod from Hess Deep, equatorial Pacific: A comparison between abyssal and alpine-type podiform chromitites. *Lithos*, *43*, 1–14. https://doi.org/10.1016/s0024-4937(98)00003-6

Arai, S., & Yurimoto, H. (1994). Podiform chromitites of the Tari-Misaka ultramafic complex, southwestern Japan, as mantle-melt interaction products. *Economic Geology*, *89*(6), 1279–1288. https://doi.org/10.2113/gsecongeo.89.6.1279

Arculus, R. J., Gurnis, M., Ishizuka, O., Reagan, M. K., Pearce, J. A., & Sutherland, R. (2019). How to create new Subduction zones. *Oceanography*, *32*(1), 160–174. https://doi.org/10.5670/oceanog.2019.140

Benton, L. D., Ryan, J. G., & Savov, I. P. (2004). Lithium abundance and isotope systematics of forearc serpentinites, Conical Seamount, Mariana forearc: Insights into the mechanics of slab-mantle exchange during subduction. *Geochemistry, Geophysics, Geosystems*, *5*(8). https://doi.org/10.1029/2004GC000708

Boudier, F., & Nicolas, A. (1995). Nature of the Moho transition zone in the Oman ophiolite. *Journal of Petrology*, *36*(3), 777–796. https://doi.org/10.1093/petrology/36.3.777

Braun, M. G., & Kelemen, P. B. (2002). Dunite distribution in the Oman ophiolite: Implications for melt flux through porous dunite conduits. *Geochemistry, Geophysics, Geosystems*, *3*(11), 1–21. https://doi.org/10.1029/2001gc000289

Brenan, J. M., Neroda, E., Lundstrom, C. C., Shaw, H. F., Ryerson, F. J., & Phinney, D. L. (1998). Behaviour of boron, beryllium, and lithium during melting and crystallization: Constraints from mineral-melt partitioning experiments. *Geochimica et Cosmochimica Acta*, *62*(12), 2129–2141. https://doi.org/10.1016/s0016-7037(98)00131-8

Cameron, W. E., Nisbet, E. G., & Dietrich, V. J. (1979). Boninites, komatiites and ophiolitic basalts. *Nature*, *280*(5723), 550–553. https://doi.org/10.1038/280550a0

Casey, J. F., & Dewey, J. F. (1984). Initiation of subduction zones along transform and accreting plate boundaries, triple-junction evolution, and forearc spreading centres—Implications for ophiolitic geology and obduction. *Geological Society, London, Special Publications*, *13*(1), 269–290. https://doi.org/10.1144/gsl.sp.1984.013.01.22

Chan, L. H., Edmond, J. M., Thompson, G., & Gillis, K. (1992). Lithium isotopic composition of submarine basalts: Implications for the lithium cycle in the oceans. *Earth and Planetary Science Letters*, *108*(1–3), 151–160. https://doi.org/10.1016/0012-821x(92)90067-6

Chan, L. H., Leeman, W. P., & You, C. F. (2002). Lithium isotopic composition of Central American volcanic arc lavas: Implications for modification of subarc mantle by slab-derived fluids: Correction. *Chemical Geology*, *182*(2–4), 293–300. https://doi.org/10.1016/s0009-2541(01)00298-4

Chen, C., Su, B. X., Xiao, Y., Pang, K. N., Robinson, P. T., Uysal, I., et al. (2019). Intermediate chromitite in Kızıldağ ophiolite (SE Turkey) formed during subduction initiation in Neo-Tethys. *Ore Geology Reviews*, *104*, 88–100. https://doi.org/10.1016/j.oregeorev.2018.10.004

Coogan, L. A., Jenkin, G. R. T., & Wilson, R. N. (2007). Contrasting cooling rates in the lower oceanic crust at fast-and slow-spreading ridges revealed by geospeedometry. *Journal of Petrology*, *48*(11), 2211–2231. https://doi.org/10.1093/petrology/egm057

Dick, H. J., Lin, J., & Schouten, H. (2003). An ultraslow-spreading class of ocean ridge. *Nature*, *426*(6965), 405–412. https://doi.org/10.1038/nature02128

Dilek, Y., & Thy, P. (2009). Island arc tholeiite to boninitic melt evolution of the Cretaceous Kizildag (Turkey) ophiolite: Model for multi-stage early arc–forearc magmatism in Tethyan subduction factories. *Lithos*, *113*(1–2), 68–87. https://doi.org/10.1016/j.lithos.2009.05.044

Dohmen, R., Kasemann, S. A., Coogan, L., & Chakraborty, S. (2010). Diffusion of Li in olivine. Part I: Experimental observations and a multi species diffusion model. *Geochimica et Cosmochimica Acta*, *74*(1), 274–292. https://doi.org/10.1016/j.gca.2009.10.016

Dubois-Côté, V., Hébert, R., Dupuis, C., Wang, C. S., Li, Y. L., & Dostal, J. (2005). Petrological and geochemical evidence for the origin of the Yarlung Zangbo ophiolites, southern Tibet. *Chemical Geology*, *214*(3–4), 265–286. https://doi.org/10.1016/j.chemgeo.2004.10.004

Elliott, T., Jeffcoate, A., & Bouman, C. (2004). The terrestrial Li isotope cycle: Light-weight constraints on mantle convection. *Earth and Planetary Science Letters*, *220*(3–4), 231–245. https://doi.org/10.1016/s0012-821x(04)00096-2

Encarnación, J., Mukasa, S. B., & Evans, C. A. (1999). Subduction components and the generation of arc-like melts in the Zambales ophiolite, Philippines: Pb, Sr and Nd isotopic constraints. *Chemical Geology*, *156*(1–4), 343–357. https://doi.org/10.1016/s0009-2541(98)00190-9

Encarnación, J. P., Mukasa, S. B., & Obille, E. C., Jr. (1993). Zircon U-Pb geochronology of the Zambales and Angat Ophiolites, Luzon, Philippines: Evidence for an Eocene arc-back arc pair. *Journal of Geophysical Research: Solid Earth*, *98*(B11), 19991–20004. https://doi.org/10.1029/93jb02167

Falloon, T. J., & Danyushevsky, L. V. (2000). Melting of refractory mantle at 1.5, 2 and 2.5 Gpa under anhydrous and H_2O-undersaturated conditions: Implications for the petrogenesis of high-Ca boninites and the influence of subduction components on mantle melting. *Journal of Petrology*, *41*, 257–283. https://doi.org/10.1093/petrology/41.2.257

Franz, L., & Wirth, R. (1997). Thin intergranular melt films and melt pockets in spinel peridotite xenoliths from the Rhön area (Germany): Early stage of melt generation by grain boundary melting. *Contributions to Mineralogy and Petrology*, *129*(4), 268–283. https://doi.org/10.1007/s004100050337

Gao, Y., Snow, J. E., Casey, J. F., & Yu, J. (2011). Cooling-induced fractionation of mantle Li isotopes from the ultraslow-spreading Gakkel Ridge. *Earth and Planetary Science Letters*, *301*(1–2), 231–240. https://doi.org/10.1016/j.epsl.2010.11.003

Geary, E. E., Kay, R. W., Reynolds, J. C., & Kay, S. M. (1989). Geochemistry of mafic rocks from the Coto Block, Zambales ophiolite, Philippines: Trace element evidence for two stages of crustal growth. *Tectonophysics*, *168*(1–3), 43–63. https://doi.org/10.1016/0040-1951(89)90368-5

Ghosh, B., Morishita, T., Gupta, B. S., Tamura, A., Arai, S., & Bandyopadhyay, D. (2014). Moho transition zone in the Cretaceous Andaman ophiolite, India: A passage from the mantle to the crust. *Lithos*, *198*, 117–128. https://doi.org/10.1016/j.lithos.2014.03.027

Golowin, R., Portnyagin, M., Hoernle, K., Sobolev, A., Kuzmin, D., & Werner, R. (2017). The role and conditions of second-stage mantle melting in the generation of low-Ti tholeiites and boninites: The case of the Manihiki Plateau and the Troodos ophiolite. *Contributions to Mineralogy and Petrology*, *172*(11–12), 104. https://doi.org/10.1007/s00410-017-1424-3

González-Jiménez, J. M., Proenza, J. A., Gervilla, F., Melgarejo, J. C., Blanco-Moreno, J. A., Ruiz-Sánchez, R., & Griffin, W. L. (2011). High-Cr and high-Al chromitites from the Sagua de Tánamo district, Mayarí-Cristal ophiolitic massif (eastern Cuba): Constraints on their origin from mineralogy and geochemistry of chromian spinel and platinum-group elements. *Lithos*, *125*(1–2), 101–121. https://doi.org/10.1016/j.lithos.2011.01.016

Gordeychik, B., Churikova, T., Kronz, A., Sundermeyer, C., Simakin, A., & Wörner, G. (2018). Growth of, and diffusion in, olivine in ultra-fast ascending basalt magmas from Shiveluch volcano. *Scientific Reports*, *8*, 1–15. https://doi.org/10.1038/s41598-018-30133-1

Green, D. H., & Falloon, T. J. (2015). Mantle-derived magmas: Intraplate, hot-spots and mid-ocean ridges. *Science Bulletin*, *60*(22), 1873–1900. https://doi.org/10.1007/s11434-015-0920-y

Halama, R., Savov, I. P., Rudnick, R. L., & McDonough, W. F. (2009). Insights into Li and Li isotope cycling and sub-arc metasomatism from veined mantle xenoliths, Kamchatka. *Contributions to Mineralogy and Petrology*, *158*(2), 197–222. https://doi.org/10.1007/s00410-009-0378-5

He, L. (2014). Numerical modeling of convective erosion and peridotite-melt interaction in big mantle wedge: Implications for the destruction of the North China Craton. *Journal of Geophysical Research: Solid Earth*, *119*(4), 3662–3677. https://doi.org/10.1002/2013jb010657

Hirose, K., & Kawamoto, T. (1995). Hydrous partial melting of lherzolite at 1 GPa: The effect of H_2O on the genesis of basaltic magmas. *Earth and Planetary Science Letters*, *133*(3–4), 463–473. https://doi.org/10.1016/0012-821x(95)00096-u

Hock, M., Friedrich, G., Plüger, W. L., & Wichowski, A. (1986). Refractory-and metallurgical-type chromite ores, Zambales ophiolite, Luzon, Philippines. *Mineralium Deposita*, *21*(3), 190–199. https://doi.org/10.1007/bf00199799

Ishikawa, T., Fujisawa, S., Nagaishi, K., & Masuda, T. (2005). Trace element characteristics of the fluid liberated from amphibolite-facies slab: Inference from the metamorphic sole beneath the Oman ophiolite and implication for boninite genesis. *Earth and Planetary Science Letters*, *240*(2), 355–377. https://doi.org/10.1016/j.epsl.2005.09.049

Ishizuka, O., Taylor, R. N., Umino, S., & Kanayama, K. (2020). Geochemical evolution of arc and slab following subduction initiation: A record from the Bonin Islands, Japan. *Journal of Petrology*, *61*(5). https://doi.org/10.1093/petrology/egaa050

Jeffcoate, A. B., Elliott, T., Kasemann, S. A., Ionov, D., Cooper, K., & Brooker, R. (2007). Li isotope fractionation in peridotites and mafic melts. *Geochimica et Cosmochimica Acta*, *71*(1), 202–218. https://doi.org/10.1016/j.gca.2006.06.1611

Kamenetsky, V. S., Crawford, A. J., & Meffre, S. (2001). Factors controlling chemistry of magmatic spinel: An empirical study of associated olivine, Cr-spinel and melt inclusions from primitive rocks. *Journal of Petrology*, *42*(4), 655–671. https://doi.org/10.1093/petrology/42.4.655

Kelemen, P. B. (1990). Reaction between ultramafic rock and fractionating basaltic magma I. Phase relations, the origin of calc-alkaline magma series, and the formation of discordant dunite. *Journal of Petrology*, *31*(1), 51–98. https://doi.org/10.1093/petrology/31.1.51

Kelemen, P. B., Dick, H. J., & Quick, J. E. (1992). Formation of harzburgite by pervasive melt/rock reaction in the upper mantle. *Nature*, *358*(6388), 635–641. https://doi.org/10.1038/358635a0

Klingenberg, B. M. E. T., & Kushiro, I. (1996). Melting of a chromite-bearing harzburgite and generation of boninitic melts at low pressures under controlled oxygen fugacity. *Lithos*, *37*, 1–14. https://doi.org/10.1016/0024-4937(95)00025-9

Kushiro, I. (2001). Partial melting experiments on peridotite and origin of mid-ocean ridge basalt. *Annual Review of Earth and Planetary Sciences*, *29*(1), 71–107. https://doi.org/10.1146/annurev.earth.29.1.71

Lai, Y. J., von Strandmann, P. A. P., Dohmen, R., Takazawa, E., & Elliott, T. (2015). The influence of melt infiltration on the Li and Mg isotopic composition of the Horoman Peridotite Massif. *Geochimica et Cosmochimica Acta*, *164*, 318–332. https://doi.org/10.1016/j.gca.2015.05.006

Leblanc, M., & Violette, J. F. (1983). Distribution of aluminum-rich and chromium-rich chromite pods in ophiolite peridotites. *Economic Geology*, *78*(2), 293–301. https://doi.org/10.2113/gsecongeo.78.2.293

Liang, Y., & Elthon, D. (1990). Evidence from chromium abundances in mantle rocks for extraction of picrite and komatiite melts. *Nature*, *343*(6258), 551–553. https://doi.org/10.1038/343551a0

Liu, C. Z., Wu, F. Y., Liu, T., Zhang, C., Zhang, W. Q., Zhang, Z. Y., et al. (2022). An origin of ultraslow spreading ridges for the Yarlung-Tsangpo ophiolites. *Fundamental Research*, *2*(1), 74–83. https://doi.org/10.1016/j.fmre.2021.07.002

Liu, P. P., Liang, J., Dick, H. J., Li, X. H., Chen, Q., Zuo, H. Y., & Wu, J. C. (2020). Enormous lithium isotopic variations of abyssal peridotites reveal fast cooling and melt/fluid-rock interactions. *Journal of Geophysical Research: Solid Earth*, *125*, e2020JB020393. https://doi.org/10.1029/2020JB020393

Liu, X., Su, B. X., Xiao, Y., Chen, C., Uysal, I., Jing, J. J., et al. (2019). Initial subduction of Neo-Tethyan ocean: Geochemical records in chromite and mineral inclusions in the Pozantı-Karsantı ophiolite, southern Turkey. *Ore Geology Reviews*, *110*, 102926. https://doi.org/10.1016/j.oregeorev.2019.05.012

Lundstrom, C. C., Chaussidon, M., Hsui, A. T., Kelemen, P., & Zimmerman, M. (2005). Observations of Li isotopic variations in the Trinity Ophiolite: Evidence for isotopic fractionation by diffusion during mantle melting. *Geochimica et Cosmochimica Acta*, *69*(3), 735–751. https://doi.org/10.1016/j.gca.2004.08.004

Marchesi, C., Garrido, C. J., Godard, M., Proenza, J. A., Gervilla, F., & Blanco-Moreno, J. (2006). Petrogenesis of highly depleted peridotites and gabbroic rocks from the Mayarí-Baracoa Ophiolitic Belt (eastern Cuba). *Contributions to Mineralogy and Petrology*, *151*(6), 717–736. https://doi.org/10.1007/s00410-006-0089-0

Marschall, H. R., Pogge von Strandmann, P. A. E., Seitz, H. M., Elliott, T., & Niu, Y. (2007). The lithium isotopic composition of orogenic eclogites and deep subducted slabs. *Earth and Planetary Science Letters*, *262*(3–4), 563–580. https://doi.org/10.1016/j.epsl.2007.08.005

Marschall, H. R., & Tang, M. (2020). High-temperature processes: Is it time for lithium isotopes? *Elements*, *16*(4), 247–252. https://doi.org/10.2138/gselements.16.4.247

Marschall, H. R., Wanless, V. D., Shimizu, N., Von Strandmann, P. A. P., Elliott, T., & Monteleone, B. D. (2017). The boron and lithium isotopic composition of mid-ocean ridge basalts and the mantle. *Geochimica et Cosmochimica Acta*, *207*, 102–138. https://doi.org/10.1016/j.gca.2017.03.028

Matsukage, K. N., & Kubo, K. (2003). Chromian spinel during melting experiments of dry peridotite (KLB-1) at 1.0–2.5 GPa. *American Mineralogist*, *88*(8–9), 1271–1278. https://doi.org/10.2138/am-2003-8-909

Maunder, B., Prytulak, J., Goes, S., & Reagan, M. (2020). Rapid subduction initiation and magmatism in the Western Pacific driven by internal vertical forces. *Nature Communication*, *11*, 1–8. https://doi.org/10.1038/s41467-020-15737-4

McKenzie, D., Jackson, J., & Priestley, K. (2005). Thermal structure of oceanic and continental lithosphere. *Earth and Planetary Science Letters*, *233*(3–4), 337–349. https://doi.org/10.1016/j.epsl.2005.02.005

Melcher, F., Grum, W., Simon, G., Thalhammer, T. V., & Stumpfl, E. F. (1997). Petrogenesis of the ophiolitic giant chromite deposits of Kempirsai, Kazakhstan: A study of solid and fluid inclusions in chromite. *Journal of Petrology*, *38*(10), 1419–1458. https://doi.org/10.1093/petroj/38.10.1419

Moriguti, T., & Nakamura, E. (1998). Across-arc variation of Li isotopes in lavas and implications for crust/mantle recycling at subduction zones. *Earth and Planetary Science Letters*, *163*(1–4), 167–174. https://doi.org/10.1016/s0012-821x(98)00184-8

Morishita, T., Maeda, J., Miyashita, S., Kumagai, H., Matsumoto, T., & Dick, H. J. (2007). Petrology of local concentration of chromian spinel in dunite from the slow-spreading Southwest Indian Ridge. *European Journal of Mineralogy*, *19*(6), 871–882. https://doi.org/10.1127/0935-1221/2007/0019-1773

Morishita, T., Tani, K., Shukuno, H., Harigane, Y., Tamura, A., Kumagai, H., & Hellebrand, E. (2011). Diversity of melt conduits in the Izu-Bonin-Mariana forearc mantle: Implications for the earliest stage of arc magmatism. *Geology*, *39*(4), 411–414. https://doi.org/10.1130/g31706.1

Niu, Y., & Batiza, R. (1991). In situ densities of MORB melts and residual mantle: Implications for buoyancy forces beneath mid-ocean ridges. *The Journal of Geology*, *99*(5), 767–775. https://doi.org/10.1086/629538

O'Reilly, S. Y., Chen, D., Griffin, W. L., & Ryan, C. G. (1997). Minor elements in olivine from spinel lherzolite xenoliths: Implications for thermobarometry. *Mineralogical Magazine*, *61*(405), 257–269. https://doi.org/10.1180/minmag.1997.061.405.09

Ottolini, L., Laporte, D., Raffone, N., Devidal, J. L., & Le Fèvre, B. (2009). New experimental determination of Li and B partition coefficients during upper mantle partial melting. *Contributions to Mineralogy and Petrology*, *157*(3), 313–325. https://doi.org/10.1007/s00410-008-0336-7

Ottolini, L., Le Fèvre, B., & Vannucci, R. (2004). Direct assessment of mantle boron and lithium contents and distribution by SIMS analyses of peridotite minerals. *Earth and Planetary Science Letters*, *228*(1–2), 19–36. https://doi.org/10.1016/j.epsl.2004.09.027

Ozawa, K. (1983). Evaluation of olivine-spinel geothermometry as an indicator of thermal history for peridotites. *Contributions to Mineralogy and Petrology*, *82*(1), 52–65. https://doi.org/10.1007/bf00371175

Parkinson, I. J., Hammond, S. J., James, R. H., & Rogers, N. W. (2007). High-temperature lithium isotope fractionation: Insights from lithium isotope diffusion in magmatic systems. *Earth and Planetary Science Letters*, *257*(3–4), 609–621. https://doi.org/10.1016/j.epsl.2007.03.023

Patriat, M., Falloon, T., Danyushevsky, L. V., Collot, J., Jean, M. M., Hoernle, K., et al. (2019). Subduction initiation terranes at the front of a 2 Ma volcanically-active subduction zone. *Earth and Planetary Science Letters*, *508*, 30–40. https://doi.org/10.1016/j.epsl.2018.12.011

Payot, B. D., Arai, S., Tamayo, R. A., Jr., & Yumul, G. P., Jr. (2013). Textural evidence for the chromite-oversaturated character of the melt involved in podiform chromitite formation. *Resource Geology*, *63*(3), 313–319. https://doi.org/10.1111/rge.12011

Pearce, J. A. (2003). Supra-subduction zone ophiolites: The search for modern analogues. *Special Papers - Geological Society of America*, *373*, 269–294.

Pearce, J. A., Barker, P. F., Edwards, S. J., Parkinson, I. J., & Leat, P. T. (2000). Geochemistry and tectonic significance of peridotites from the South Sandwich arc–basin system, South Atlantic. *Contributions to Mineralogy and Petrology*, *139*(1), 36–53. https://doi.org/10.1007/s004100050572

Perez, A., Umino, S., Yumul, G. P., Jr., & Ishizuka, O. (2018). Boninite and boninite-series volcanics in northern Zambales ophiolite: Doubly vergent subduction initiation along Philippine Sea plate margins. *Solid Earth*, *9*(3), 713–733. https://doi.org/10.5194/se-9-713-2018

Pogge von Strandmann, P. A. E., Elliott, T., Marschall, H. R., Coath, C., Lai, Y. J., Jeffcoate, A. B., & Ionov, D. A. (2011). Variations of Li and Mg isotope ratios in bulk chondrites and mantle xenoliths. *Geochimica et Cosmochimica Acta*, *75*(18), 5247–5268. https://doi.org/10.1016/j.gca.2011.06.026

Portnyagin, M., Hoernle, K., & Savelyev, D. (2009). Ultra-depleted melts from Kamchatkan ophiolites: Evidence for the interaction of the Hawaiian plume with an oceanic spreading center in the Cretaceous? *Earth and Planetary Science Letters*, *287*(1–2), 194–204. https://doi.org/10.1016/j.epsl.2009.07.042

Queaño, K. L., Dimalanta, C. B., Yumul, G. P., Jr., Marquez, E. J., Faustino-Eslava, D. V., Suzuki, S., & Ishida, K. (2017). Stratigraphic units overlying the Zambales Ophiolite complex (ZOC) in Luzon, (Philippines): Tectonostratigraphic significance and regional implications. *Journal of Asian Earth Sciences*, *142*, 20–31. https://doi.org/10.1016/j.jseaes.2016.06.011

Reagan, M. K., Heaton, D. E., Schmitz, M. D., Pearce, J. A., Shervais, J. W., & Koppers, A. A. (2019). Forearc ages reveal extensive short-lived and rapid seafloor spreading following subduction initiation. *Earth and Planetary Science Letters*, *506*, 520–529. https://doi.org/10.1016/j.epsl.2018.11.020

Reagan, M. K., Ishizuka, O., Stern, R. J., Kelley, K. A., Ohara, Y., Blichert-Toft, J., et al. (2010). Forearc basalts and subduction initiation in the Izu-Bonin-Mariana system. *Geochemistry, Geophysics, Geosystems*, *11*(3). https://doi.org/10.1029/2009GC002871

Reagan, M. K., Pearce, J. A., Petronotis, K., Almeev, R. R., Avery, A. J., Carvallo, C., et al. (2017). Subduction initiation and ophiolite crust: New insights from IODP drilling. *International Geology Review*, *59*(11), 1439–1450. https://doi.org/10.1080/00206814.2016.1276482

Richter, F., Watson, B., Chaussidon, M., Mendybaev, R., & Ruscitto, D. (2014). Lithium isotope fractionation by diffusion in minerals. Part 1: Pyroxenes. *Geochimica et Cosmochimica Acta*, *126*, 352–370. https://doi.org/10.1016/j.gca.2013.11.008

Robertson, A., Parlak, O., Ustaömer, T., Taslı, K., İnan, N., Dumitrica, P., & Karaoğlan, F. (2013). Subduction, ophiolite genesis and collision history of Tethys adjacent to the Eurasian continental margin: New evidence from the Eastern Pontides, Turkey. *Geodinamica Acta*, *26*(3–4), 230–293. https://doi.org/10.1080/09853111.2013.877240

Robinson, P. T., Zhou, M. F., Hu, X. F., Reynolds, P., Bai, W. J., & Yang, J. (1999). Geochemical constraints on the origin of the Hegenshan ophiolite, Inner Mongolia, China. *Journal of Asian Earth Sciences*, *17*(4), 423–442. https://doi.org/10.1016/s1367-9120(99)00016-4

Rollinson, H. (2008). The geochemistry of mantle chromitites from the northern part of the Oman ophiolite: Inferred parental melt compositions. *Contributions to Mineralogy and Petrology*, *156*(3), 273–288. https://doi.org/10.1007/s00410-008-0284-2

Rudnick, R. L., & Ionov, D. A. (2007). Lithium elemental and isotopic disequilibrium in minerals from peridotite xenoliths from far-east Russia: Product of recent melt/fluid–rock reaction. *Earth and Planetary Science Letters*, *256*(1–2), 278–293. https://doi.org/10.1016/j.epsl.2007.01.035

Savov, I. P., Ryan, J. G., D'Antonio, M., & Fryer, P. (2007). Shallow slab fluid release across and along the Mariana arc-basin system: Insights from geochemistry of serpentinized peridotites from the Mariana fore arc. *Journal of Geophysical Research: Solid Earth*, *112*(B9), B09205. https://doi.org/10.1029/2006JB004749

Schmitt, A. K., Perfit, M. R., Rubin, K. H., Stockli, D. F., Smith, M. C., Cotsonika, L. A., et al. (2011). Rapid cooling rates at an active mid-ocean ridge from zircon thermochronology. *Earth and Planetary Science Letters*, *302*(3–4), 349–358. https://doi.org/10.1016/j.epsl.2010.12.022

Schwartz, J. J., John, B. E., Cheadle, M. J., Miranda, E. A., Grimes, C. B., Wooden, J. L., & Dick, H. J. (2005). Dating the growth of oceanic crust at a slow-spreading ridge. *Science*, *310*(5748), 654–657. https://doi.org/10.1126/science.1116349

Seitz, H. M., & Woodland, A. B. (2000). The distribution of lithium in peridotitic and pyroxenitic mantle lithologies—An indicator of magmatic and metasomatic processes. *Chemical Geology*, *166*(1–2), 47–64. https://doi.org/10.1016/s0009-2541(99)00184-9

Seyler, M., Lorand, J. P., Dick, H. J., & Drouin, M. (2007). Pervasive melt percolation reactions in ultra-depleted refractory harzburgites at the Mid-Atlantic Ridge, 15 20′ N: ODP Hole 1274A. *Contributions to Mineralogy and Petrology*, *153*(3), 303–319. https://doi.org/10.1007/s00410-006-0148-6

Shervais, J. W., Reagan, M., Haugen, E., Almeev, R. R., Pearce, J. A., Prytulak, J., et al. (2019). Magmatic response to subduction initiation: Part 1. Fore-arc basalts of the Izu-Bonin arc from IODP Expedition 352. *Geochemistry, Geophysics, Geosystems*, *20*, 314–338. https://doi.org/10.1029/2018gc007731

Sigurdsson, H., & Schilling, J. G. (1976). Spinels in Mid-Atlantic Ridge basalts: Chemistry and occurrence. *Earth and Planetary Science Letters*, *29*(1), 7–20. https://doi.org/10.1016/0012-821x(76)90021-2

Sigurdsson, I. A., Kamenetsky, V. S., Crawford, A. J., Eggins, S. M., & Zlobin, S. K. (1993). Primitive island arc and oceanic lavas from the Hunter ridge-Hunter fracture zone. Evidence from glass, olivine and spinel compositions. *Mineralogy and Petrology*, *47*(2–4), 149–169. https://doi.org/10.1007/bf01161564

Stern, R. J. (2004). Subduction initiation: Spontaneous and induced. *Earth and Planetary Science Letters*, *226*(3–4), 275–292. https://doi.org/10.1016/s0012-821x(04)00498-4

Stern, R. J., Reagan, M., Ishizuka, O., Ohara, Y., & Whattam, S. (2012). To understand subduction initiation, study forearc crust: To understand forearc crust, study ophiolites. *Lithosphere*, *4*(6), 469–483. https://doi.org/10.1130/l183.1

Su, B., Zhang, H., Sakyi, P. A., Qin, K., Liu, P., Ying, J., et al. (2010). Formation of melt pocket in mantle peridotite xenolith from western Qinling, Central China: Partial melting and metasomatism. *Journal of Earth Science*, *21*(5), 641–668. https://doi.org/10.1007/s12583-010-0116-y

Su, B., Zhou, M., Jing, J., Robinson, P. T., Chen, C., Xiao, Y., et al. (2019). Distinctive melt activity and chromite mineralization in Luobusa and Purang ophiolites, southern Tibet: Constraints from trace element compositions of chromite and olivine. *Science Bulletin*, *64*(2), 108–121. https://doi.org/10.1016/j.scib.2018.12.018

Su, B. X., Bai, Y., Cui, M. M., Wang, J., Xiao, Y., Lenaz, D., et al. (2020). Petrogenesis of the Ultramafic Zone of the Stillwater Complex in North America: Constraints from mineral chemistry and stable isotopes of Li and O. *Contributions to Mineralogy and Petrology*, *175*(7), 1–20. https://doi.org/10.1007/s00410-020-01707-y

Su, B. X., Gu, X. Y., Deloule, E., Zhang, H. F., Li, Q. L., Li, X. H., et al. (2015). Potential orthopyroxene, clinopyroxene and olivine reference materials for in situ lithium isotope determination. *Geostandards and Geoanalytical Research*, *39*(3), 357–369. https://doi.org/10.1111/j.1751-908x.2014.00313.x

Su, B. X., Zhou, M. F., & Robinson, P. T. (2016). Extremely large fractionation of Li isotopes in a chromitite-bearing mantle sequence. *Scientific Reports*, *6*(1), 22370. https://doi.org/10.1038/srep22370

Tang, Y. J., Zhang, H. F., & Ying, J. F. (2010). A brief review of isotopically light Li–a feature of the enriched mantle? *International Geology Review*, *52*(9), 964–976. https://doi.org/10.1080/00206810903211385

Tomascak, P. B., Langmuir, C. H., le Roux, P. J., & Shirey, S. B. (2008). Lithium isotopes in global mid-ocean ridge basalts. *Geochimica et Cosmochimica Acta*, *72*(6), 1626–1637. https://doi.org/10.1016/j.gca.2007.12.021

Tomascak, P. B., Magna, T., & Dohmen, R. (2016). *Advances in lithium isotope geochemistry*. Springer International Publishing.

Tomascak, P. B., Ryan, J. G., & Defant, M. J. (2000). Lithium isotope evidence for light element decoupling in the Panama subarc mantle. *Geology*, *28*(6), 507–510. https://doi.org/10.1130/0091-7613(2000)28<507:liefle>2.0.co;2

Tomascak, P. B., Tera, F., Helz, R. T., & Walker, R. J. (1999). The absence of lithium isotope fractionation during basalt differentiation: New measurements by multi-collector sector ICP-MS. *Geochimica et Cosmochimica Acta*, *63*(6), 907–910. https://doi.org/10.1016/s0016-7037(98)00318-4

Tomascak, P. B., Widom, E., Benton, L. D., Goldstein, S. L., & Ryan, J. G. (2002). The control of lithium budgets in island arcs. *Earth and Planetary Science Letters*, *196*(3–4), 227–238. https://doi.org/10.1016/s0012-821x(01)00614-8

Ueda, K., Gerya, T., & Sobolev, S. V. (2008). Subduction initiation by thermal–chemical plumes: Numerical studies. *Earth and Planetary Physics*, *171*, 296–312.

Uysal, İ., Ersoy, E. Y., Karslı, O., Dilek, Y., Sadıklar, M. B., Ottley, C. J., et al. (2012). Coexistence of abyssal and ultra-depleted SSZ type mantle peridotites in a Neo-Tethyan Ophiolite in SW Turkey: Constraints from mineral composition, whole-rock geochemistry (major–trace–REE–PGE), and Re–Os isotope systematics. *Lithos*, *132*, 50–69. https://doi.org/10.1016/j.lithos.2011.11.009

Uysal, I., Tarkian, M., Sadiklar, M. B., Zaccarini, F., Meisel, T., Garuti, G., & Heidrich, S. (2009). Petrology of Al-and Cr-rich ophiolitic chromitites from the Muğla, SW Turkey: Implications from composition of chromite, solid inclusions of platinum-group mineral, silicate, and base-metal mineral, and Os-isotope geochemistry. *Contributions to Mineralogy and Petrology*, *158*(5), 659–674. https://doi.org/10.1007/s00410-009-0402-9

Waldman, R. J., Marsaglia, K. M., Hickey-Vargas, R., Ishizuka, O., Johnson, K. E., McCarthy, A., et al. (2021). Sedimentary and volcanic record of the nascent Izu-Bonin-Mariana arc from IODP Site U1438. *Geological Society of America Bulletin*, *133*(7–8), 1421–1440. https://doi.org/10.1130/b35612.1

Wang, J., Su, B. X., Robinson, P. T., Xiao, Y., Bai, Y., Liu, X., et al. (2021). Trace elements in olivine: Proxies for petrogenesis, mineralization and discrimination of mafic-ultramafic rocks. *Lithos*, *388*, 106085. https://doi.org/10.1016/j.lithos.2021.106085

Whattam, S. A., & Stern, R. J. (2011). The 'subduction initiation rule': A key for linking ophiolites, intra-oceanic forearcs, and subduction initiation. *Contributions to Mineralogy and Petrology*, *162*(5), 1031–1045. https://doi.org/10.1007/s00410-011-0638-z

Wu, J., Suppe, J., Lu, R., & Kanda, R. (2016). Philippine Sea and East Asian plate tectonics since 52 Ma constrained by new subducted slab reconstruction methods. *Journal of Geophysical Research: Solid Earth*, *121*(6), 4670–4741. https://doi.org/10.1002/2016jb012923

Xiong, F. H., Yang, J. S., & Liu, Z. (2013). Multi-satge formation of the podiform chromitite. *Geology in China*, *40*, 820–839. (in Chinese with English Abstract).

Xiong, F. H., Yang, J. S., Robinson, P. T., Xu, X., Liu, Z., Zhou, W., et al. (2017). High-Al and high-Cr podiform chromitites from the western Yarlung-Zangbo suture zone, Tibet: Implications from mineralogy and geochemistry of chromian spinel, and platinum-group elements. *Ore Geology Reviews*, *80*, 1020–1041. https://doi.org/10.1016/j.oregeorev.2016.09.009

Yu, M. M. (2015). The geochemical characteristics and its tectonic significance of the ophiolites from the Zambales Range, Luzon, Philippines. Master degree thesis of the University of Chinese Academy of Sciences (pp. 78–81).

Yumul, G. P., Jr. (1996). Varying mantle sources of supra-subduction zone ophiolites: REE evidence from the Zambales ophiolite complex, Luzon, Philippines. *Tectonophysics*, *262*(1–4), 243–262. https://doi.org/10.1016/0040-1951(96)00013-3

Yumul, G. P., Jr. (2004). Zambales Ophiolite complex (Philippines) transition-zone dunites: Restite, cumulate, or replacive products? *International Geology Review*, *46*(3), 259–272. https://doi.org/10.2747/0020-6814.46.3.259

Yumul, G. P., Jr., Dimalanta, C. B., Faustino, D. V., & De Jesus, J. V. (1998). Translation and docking of an arc terrane: Geological and geochemical evidence from the southern Zambales Ophiolite Complex, Philippines. *Tectonophysics*, *293*(3–4), 255–272. https://doi.org/10.1016/s0040-1951(98)00096-1

Yumul, G. P., Jr., Dimalanta, C. B., Salapare, R. C., Queaño, K. L., Faustino-Eslava, D. V., Marquez, E. J., et al. (2020). Slab rollback and microcontinent subduction in the evolution of the Zambales Ophiolite Complex (Philippines): A review. *Geoscience Frontiers*, *11*(1), 23–36. https://doi.org/10.1016/j.gsf.2018.12.008

Zhang, P. F., Uysal, I., Zhou, M. F., Su, B. X., & Avcı, E. (2016). Subduction initiation for the formation of high-Cr chromitites in the Kop ophiolite, NE Turkey. *Lithos*, *260*, 345–355. https://doi.org/10.1016/j.lithos.2016.05.025

Zhang, P. F., Zhou, M. F., Liu, Q. Y., Malpas, J., Robinson, P. T., & He, Y. S. (2019a). Modification of mantle rocks by plastic flow below spreading centers: Fe isotopic and fabric evidence from the Luobusa ophiolite, Tibet. *Geochimica et Cosmochimica Acta*, *253*, 84–110. https://doi.org/10.1016/j.gca.2019.03.008

Zhang, P. F., Zhou, M. F., Robinson, P. T., Pearce, J. A., Malpas, J., Liu, Q. Y., & Xia, X. P. (2019). Evolution of nascent mantle wedges during subduction initiation: Li-O isotopic evidence from the Luobusa ophiolite, Tibet. *Geochimica et Cosmochimica Acta*, *245*, 35–58. https://doi.org/10.1016/j.gca.2018.09.037

Zhang, P. F., Zhou, M. F., Su, B. X., Uysal, I., Robinson, P. T., Avcı, E., & He, Y. S. (2017). Iron isotopic fractionation and origin of chromitites in the paleo-Moho transition zone of the Kop ophiolite, NE Turkey. *Lithos*, *268*, 65–75. https://doi.org/10.1016/j.lithos.2016.10.019

Zhang, P. F., Zhou, M. F., & Yumul, G. P., Jr. (2020). Coexistence of high-Al and high-Cr chromite orebodies in the Acoje block of the Zambales ophiolite, Philippines: Evidence for subduction initiation. *Ore Geology Reviews*, *126*, 103739. https://doi.org/10.1016/j.oregeorev.2020.103739

Zhang, P. F., Zhou, M. F., Yumul, G. P., Jr., & Wang, C. Y. (2021). Geodynamic setting of high-Cr chromite mineralization in nascent subduction zones: Li isotopic and REE constraints from the Zambales ophiolite, Philippines. *Lithos*, *384*, 105975. https://doi.org/10.1016/j.lithos.2021.105975

Zhang, Q. Z., Ba, D. Z., Xiong, F. H., & Yang, J. S. (2017). Discussion on genesis process and deep prospecting breakthrough of Luobusa chromitite, Tibet. *Geology in China*, *44*, 224–241. (in Chinese with English abstract).

Zhou, M. F., Robinson, P. T., & Bai, W. J. (1994). Formation of podiform chromitites by melt/rock interaction in the upper mantle. *Mineralium Deposita*, *29*(1), 98–101. https://doi.org/10.1007/bf03326400

Zhou, M. F., Robinson, P. T., Malpas, J., Aitchison, J., Sun, M., Bai, W. J., et al. (2001). Melt/mantle interaction and melt evolution in the Sartohay high-Al chromite deposits of the Dalabute ophiolite (NW China). *Journal of Asian Earth Sciences*, *19*(4), 517–534. https://doi.org/10.1016/s1367-9120(00)00048-1

Zhou, M. F., Robinson, P. T., Malpas, J., & Li, Z. (1996). Podiform chromitites in the Luobusa ophiolite (southern Tibet): Implications for melt-rock interaction and chromite segregation in the upper mantle. *Journal of Petrology*, *37*(1), 3–21. https://doi.org/10.1093/petrology/37.1.3

Zhou, M. F., Robinson, P. T., Su, B. X., Gao, J. F., Li, J. W., Yang, J. S., & Malpas, J. (2014). Compositions of chromite, associated minerals, and parental magmas of podiform chromite deposits: The role of slab contamination of asthenospheric melts in suprasubduction zone environments. *Gondwana Research*, *26*(1), 262–283. https://doi.org/10.1016/j.gr.2013.12.011

Zhou, M. F., Sun, M., Keays, R. R., & Kerrich, R. W. (1998). Controls on platinum-group elemental distributions of podiform chromitites: A case study of high-Cr and high-Al chromitites from Chinese orogenic belts. *Geochimica et Cosmochimica Acta*, *62*(4), 677–688. https://doi.org/10.1016/s0016-7037(97)00382-7

Zhou, M. F., Yumul, G. P., Malpas, J., & Sun, M. (2000). Comparative study of platinum-group elements in the Coto and Acoje blocks of the Zambales Ophiolite complex, Philippines. *Island Arc*, *9*(4), 556–564. https://doi.org/10.1111/j.1440-1738.2000.00301.x

Zhu, W., Gaetani, G. A., Fusseis, F., Montési, L. G., & De Carlo, F. (2011). Microtomography of partially molten rocks: Three-dimensional melt distribution in mantle peridotite. *Science*, *332*(6025), 88–91. https://doi.org/10.1126/science.1202221